

Alma Mater Studiorum Università di Bologna
Archivio istituzionale della ricerca

The impact of sea surface temperature biases on North American precipitation in a high-resolution climate model

This is the final peer-reviewed author's accepted manuscript (postprint) of the following publication:

Published Version:

Johnson N.C., Krishnamurthy L., Wittenberg A.T., Xiang B., Vecchi G.A., Kapnick S.B., et al. (2020). The impact of sea surface temperature biases on North American precipitation in a high-resolution climate model. JOURNAL OF CLIMATE, 33(6), 2427-2447 [10.1175/JCLI-D-19-0417.1].

Availability:

This version is available at: <https://hdl.handle.net/11585/850752> since: 2022-02-01

Published:

DOI: <http://doi.org/10.1175/JCLI-D-19-0417.1>

Terms of use:

Some rights reserved. The terms and conditions for the reuse of this version of the manuscript are specified in the publishing policy. For all terms of use and more information see the publisher's website.

This item was downloaded from IRIS Università di Bologna (<https://cris.unibo.it/>).
When citing, please refer to the published version.

(Article begins on next page)

This is the final peer-reviewed accepted manuscript of:

Johnson, N. C., L. Krishnamurthy, A. T. Wittenberg, B. Xiang, G. A. Vecchi, S. B. Kapnick, and S. Pascale, 2020: The Impact of Sea Surface Temperature Biases on North American Precipitation in a High-Resolution Climate Model. *J. Climate*, 33, 2427–2447.

The final published version is available online at: <https://doi.org/10.1175/JCLI-D-19-0417.1>

Rights / License:

The terms and conditions for the reuse of this version of the manuscript are specified in the publishing policy. For all terms of use and more information see the publisher's website.

This item was downloaded from IRIS Università di Bologna (<https://cris.unibo.it/>)

When citing, please refer to the published version.

The impact of sea surface temperature biases on North American precipitation in a high-resolution climate model

Nathaniel C. Johnson^{1,2}, Lakshmi Krishnamurthy^{1,2}, Andrew T. Wittenberg²,
Baoqiang Xiang^{2,3}, Gabriel A. Vecchi^{1,2,4}, Sarah Kapnick², and Salvatore
Pascale^{1,2,5}

¹Atmospheric and Oceanic Sciences Program, Princeton University, Princeton,
New Jersey

²National Oceanic and Atmospheric Administration/Geophysical Fluid
Dynamics Laboratory, Princeton, New Jersey

³University Corporation for Atmospheric Research, Boulder, Colorado

⁴Princeton Environmental Institute, Princeton University, Princeton, New Jersey

⁵Department of Earth System Science, Stanford University, Stanford, California

Journal of Climate

Revised November 5, 2019

Corresponding author address: Nathaniel C. Johnson, NOAA/Geophysical Fluid Dynamics Laboratory, Princeton
University Forrestal Campus, 201 Forrestal Rd., Princeton, NJ 08540-6649
E-mail: Nathaniel.Johnson@noaa.gov

ABSTRACT

Positive precipitation biases over western North America have remained a pervasive problem in the current generation of coupled global climate models. These biases are substantially reduced, however, in a version of the Geophysical Fluid Dynamics Laboratory Forecast-oriented Low Ocean Resolution (FLOR) coupled climate model with systematic sea surface temperature (SST) biases artificially corrected through flux adjustment. This study examines how the SST biases in the Atlantic and Pacific Oceans contribute to the North American precipitation biases. Experiments with the FLOR model in which SST biases are removed in the Atlantic and Pacific are carried out to determine the contribution of SST errors in each basin to precipitation statistics over North America. Tropical and North Pacific SST biases have a strong impact on northern North American precipitation, while tropical Atlantic SST biases have a dominant impact on precipitation biases in southern North America, including the western United States. Most notably, negative SST biases in the tropical Atlantic in boreal winter induce an anomalously strong Aleutian low and a southward bias in the North Pacific storm track. In boreal summer, the negative SST biases induce a strengthened North Atlantic Subtropical High and Great Plains low-level jet. Each of these impacts contributes to positive annual mean precipitation biases over western North America. Both North Pacific and North Atlantic SST biases induce SST biases in remote basins through dynamical pathways, so a complete attribution of the effects of SST biases on precipitation must account for both the local and remote impacts.

1. Introduction

Prediction of regional precipitation changes, from intraseasonal and seasonal climate forecasts to projections under global warming, remains a challenge owing to the complexity of physical processes cutting across a wide range of time and spatial scales. Consequently, state-of-the-art global climate models (GCMs) encounter persistent errors in simulating the temporal and spatial variations of precipitation (Dai 2006; Phillips and Gleckler 2006; Liu et al. 2014; Mehran et al. 2014). Pervasive and well-known biases include an unrealistic double Intertropical Convergence Zone (Mehoso et al. 1995; Lin 2007), errors in the precipitation diurnal cycle (Trenberth et al. 2003; Dai and Trenberth 2004), and the excessive production of light precipitation (Dai 2006; Sun et al. 2006; Wilcox and Donner 2007; Stephens et al. 2010). Regional climatological precipitation biases also are common. In this study, we focus on precipitation biases over North America, with emphasis on the tendency for the simulation of excessive precipitation in western North America (Phillips and Gleckler 2006; Sheffield et al. 2013; Liu et al. 2014; Mehran et al. 2014; Pascale et al. 2015; Mejia et al. 2018). Approximately 75% of all models participating in the Coupled Model Intercomparison Project phases 3 and 5 (CMIP3 and CMIP5) exhibit positive precipitation biases over the western United States (Mejia et al. 2018). This bias pattern incorporates an excessive amplitude of the annual cycle in the Pacific Northwest and the failure to capture the transition from a U.S. West Coast precipitation maximum to a Southwest minimum (Phillips and Gleckler 2006). The errors in southwestern North American precipitation relate, in part, to errors in the simulation of the North American monsoon system (NAMS), which features a peak in precipitation from July through September. GCMs typically simulate excessive NAMS precipitation amounts and season length, with both an early onset and late retreat (Geil et al. 2013; Sheffield et al. 2013).

Numerous sources likely share responsibility for the regional precipitation biases over North America, including coarse representations of topography and errors in subgrid-scale model parameterizations, like those of cloud microphysics and atmospheric convection. Common and persistent patterns of sea surface temperature (SST) biases also may play an important role by modifying the large-scale circulation and moisture transports. These common SST bias patterns include an excessively cold and westward extended Pacific cold tongue (Mehner et al. 1995; Li and Xie 2014), warm SST biases in eastern tropical and subtropical oceans (Large and Danabasoglu 2006; Richter 2015; Zuidema et al. 2016), and cold SST biases in the North Atlantic and extratropical North Pacific (Wang et al. 2014; Zhang and Zhao 2014). Multiple reasons for these common SST biases have been suggested, including errors in alongshore winds and resulting ocean upwelling, misrepresented stratocumulus cloud decks and shortwave radiation fluxes, errors in ocean eddy mixing and vertical ocean temperature gradients (Xu et al. 2014; Richter 2015; Zuidema et al. 2016), and insufficient heat transport by the Atlantic meridional overturning circulation (AMOC) (Wang et al. 2014; Zhang and Zhao 2014). Some SST biases may improve with increasing oceanic and atmospheric resolution, but many of these biases still persist even as resolution is increased to eddy-permitting and eddy-resolving scales (Delworth et al. 2012; Kirtman et al., 2012; Griffies et al. 2015; Wittenberg et al. 2018; Vecchi et al. 2019; Adcroft et al. 2019; Held et al. 2019). Attribution of regional SST biases is complicated by the potentially strong inter-basin links, as regional SST biases can induce biases in remote basins through atmospheric and oceanic pathways (Xu et al. 2014; Wang et al. 2014; Zhang et al. 2014; Zhang and Zhao 2014; Zuidema et al. 2016).

Although it is widely acknowledged that such SST biases can have important impacts on the simulation of atmospheric circulation and precipitation, few studies have provided a

comprehensive analysis of how common SST bias patterns affect the biases in other climatological features, including precipitation simulation. Several recent studies have demonstrated that Atlantic and Pacific SST biases can have far-reaching impacts on temperature, precipitation, and atmospheric circulation (Large and Danabasoglu 2006; Zhang et al. 2014; Zhang and Zhou 2014; Xu et al. 2014; Zuidema et al. 2016), although the analysis of these SST bias effects was limited. Keeley et al. (2012) performed a more targeted analysis of the effect of common North Atlantic SST biases on North Atlantic and European climate, concluding that the extratropical North Atlantic SST bias is a major cause of atmospheric circulation biases in the region. Zhang and Zhao (2014) also demonstrated that North Atlantic SST biases may induce large-scale circulation anomalies that project onto the northern annular mode, which then induce upstream climate anomalies, including SST biases in the North Pacific.

The changes in atmospheric circulation and moisture induced by SST biases also have the potential to affect the simulation of precipitation over North America. Recently, Mejia et al. (2018) performed a regional climate model study to demonstrate that typical SST biases offshore California and the Baja California Peninsula can explain a substantial fraction of the precipitation biases in the western United States. In the present study, we take a larger-scale perspective and investigate the impacts of these biases on North American climatological seasonal precipitation through the analysis of simulations from a high-resolution GCM, focusing on the impacts of both the Atlantic and Pacific SST biases and the interactions between the two basins. Approximate removal of the SST biases over the globe and in selected Atlantic and Pacific regions results in marked improvements in the simulation of North American precipitation, especially with respect to the strong zonal contrast between the western and eastern U.S. Emerging themes in this study include a dominant influence of Atlantic SST biases on the simulation of precipitation over the

U.S. and, as discussed briefly above, strong inter-basin links, whereby SST biases in the Pacific Ocean induce SST and atmospheric biases in the Atlantic, and vice versa.

2. Data and Methodology

a. Observational data

We analyze observational data primarily for the purpose of evaluating model biases, assessed for the 1951-2010 period. We estimate the observed climatological precipitation with the University of Delaware (UD) product (Willmott and Matsuura 2001), a gridded dataset at 0.5° resolution derived from station precipitation data. We assess the sensitivity of our analysis to observation precipitation dataset by performing the same calculations with Global Precipitation Climatology Centre (Schneider et al. 2014) and the Precipitation Construction over Land (Chen et al. 2002) datasets. All conclusions are insensitive to precipitation dataset, and so all results with these latter two datasets are relegated to the Supplemental Material. The climatological SST is derived from the monthly Hadley Centre Sea Ice and Sea Surface Temperature (HadISST) dataset (Rayner et al. 2003). For the storm track analyses, we use daily 500 hPa geopotential height and monthly mean 200 hPa zonal wind from the National Centers for Environmental Prediction-National Center for Atmospheric Research (NCEP/NCAR) reanalysis (Kalnay et al. 1996) for the 1976-2005 period. The 1976-2005 period is selected for comparison with the climate model control simulation with 1990 levels of radiative forcing, in contrast with the SST and precipitation bias analysis that measures against a simulation with historical levels of radiative forcing.

b. FLOR Model and Experiments

The GCM simulations analyzed in this study are generated by the Geophysical Fluid Dynamics Laboratory (GFDL) Forecast-oriented Low Ocean Resolution (FLOR) model (Vecchi et al. 2014; Wittenberg et al. 2018), a version of the Coupled Model version 2.5 (CM2.5; Delworth et al. 2012) that retains high resolution in the atmosphere and land components (approximately 50km x 50km horizontal resolution) but has lower resolution in the ocean and sea ice components (horizontal grid spacing of 1°, telescoping to 0.33° meridional spacing near the equator). Quantities are exchanged between components conservatively, by first averaging from the transmitting component's grid onto an "exchange grid" (which is the refined "overlay" of the two participating components' grids), and then onto the receiving component's grid (Balaji et al. 2006). The high atmospheric and land resolution has yielded benefits in problems ranging from subseasonal (e.g., Xiang et al. 2014, 2019; Jiang et al. 2018) to seasonal prediction (Vecchi et al. 2014; Jia et al. 2015; Yang et al. 2015; Murakami et al. 2016; Kapnick et al. 2018) and to anthropogenic climate change (Jia et al. 2016; van der Wiel et al. 2016; Pascale et al. 2017, 2018; Yang et al. 2018; Vecchi et al. 2019), although high atmospheric resolution is not a panacea (e.g., Kapnick et al. 2018). The benefit to computational efficiency from the lower ocean and sea ice resolution allows us to carry out an extensive array of experiments.

We compare the climatological precipitation characteristics in two versions of FLOR, the standard free-running version and a version for which flux adjustments are applied to bring the model's climatological SST in alignment with observations (FLOR-FA). Specifically, the flux adjustment entails modifications to the model's momentum, enthalpy, and freshwater fluxes from the atmosphere to the ocean in order to remove most of the difference between the model and

observational estimates of climatological SST and surface wind stress for the 1979-2012 period. Additional details on the flux adjustment procedure are found in Vecchi et al. (2014). Figure 1 illustrates the annual climatological precipitation over North America in FLOR, FLOR-FA, and observations, whereas Figure 2 illustrates the annual climatological SST biases in FLOR and FLOR-FA (similar SST bias patterns are found for individual seasons). All climatology and bias calculations are based on a simulation with historical estimates of radiative forcing for the 1951-2010 period. Consistent with the common biases discussed in the introduction (cf., Fig. 6 of Pascale et al. 2015), FLOR (Fig. 1b) fails to capture the amplitude of the observed (Fig. 1a) zonal gradient in climatological precipitation and simulates excessive precipitation over western North America. The climatological SST in FLOR also exhibits many of the biases discussed in the introduction (cf., Fig. 1 of Richter 2015): strong negative biases in the extratropical Pacific and Atlantic Oceans, an excessively cold Pacific cold tongue, and positive SST biases in eastern tropical and subtropical regions near continents (Fig. 2a). FLOR-FA, in contrast, performs better in simulating the sharp east-west precipitation gradient and reduces the western North American precipitation bias (Fig. 1c) (this improvement is quantified in Section 3). This distinction in climatological precipitation between FLOR and FLOR-FA holds for both cold and warm seasons and in all observational datasets analyzed (Fig. S1). As discussed above, FLOR-FA – by construction – also greatly reduces the SST biases (Fig. 2b), although the SST biases are not eliminated, particularly in extratropical regions where the biases are strongest.

In addition to the historical radiative forcing simulations, we also conduct a set of simulations with fixed radiative forcing to probe the physical processes that connect regional SST biases to global precipitation biases, as outlined in Table 1. First, we analyze years 101-200 from 200-yr control simulations (to avoid any issues with model spin-up) with radiative forcing held

fixed at 1990 values (CTL and FA for the standard and flux-adjusted simulations, respectively). The climatological differences in precipitation, SST, and atmospheric circulation between CTL and FA are very similar to the differences in the historical forcing simulations. In order to determine the roles of individual basin SST biases in the simulation of North American precipitation, we next analyze a set of 100-yr SST nudging simulations with FLOR. In these simulations, we nudge the SSTs over individual basins to the total time varying values in FA (FA climatology plus FA anomalies) with a five-day restoring timescale. This procedure nearly eliminates the SST differences with FA over individual basins while allowing free ocean/atmosphere coupling in regions where SSTs are not restored. By allowing full coupling outside the restoring regions, we can capture the influence of SST biases in one region on the SST biases in remote regions, as discussed in the introduction. Because FA has much smaller SST biases than CTL (Fig. 2), the SST restoring experiments essentially isolate the influence of SST biases in individual basins on the simulated climate.

We focus on distinguishing the influence of SST biases in the North Pacific and North Atlantic Oceans in four distinct regions (Fig. 3). In the simulation designated as TPNP, we restore total SSTs in the tropical and extratropical North Pacific basin (15°S - 60°N, 120°E to South and North American West Coast, TPNP domain hereafter) to FA values. Similarly, in the simulation designated as TANA, we restore SSTs in the tropical and extratropical North Atlantic basin (15°S - 60°N, South and North American East Coast to African and European West Coast, TANA domain hereafter) to FA values. Beyond the edges of these domains away from the coastlines, we apply a 10° buffer within which the restoring is linearly reduced to zero. To distinguish the role of tropical versus extratropical SST biases, we conduct two additional experiments in which the

restoring is only applied to the tropics (15°S - 15°N) in the Pacific and Atlantic Oceans; we designate these experiments as TP and TA, respectively.

We conduct two additional experiments with a reduced length of 50 years to investigate the roles of local and non-locally induced SST biases. Climatological precipitation and atmospheric circulation differences between experiments exhibit only small differences when comparing 50-yr and 100-yr averages (not shown), and so we conclude that 50-yr simulations are sufficient for the purposes of this study. Because SST biases in one basin can impact the biases in remote regions, we wish to distinguish the influence of the local versus the remotely forced SST biases. In the experiment designated as TPNP_{iso} (where “iso” stands for “isolated”), we restore SSTs in the TPNP domain to the FA values, just as in TPNP, but we also restore the TANA domain SSTs to CTL values. Therefore, the climatological SST differences between TPNP_{iso} and CTL are confined to the tropical and extratropical North Pacific domain, and climatological SSTs are nearly identical between TPNP_{iso} and CTL in all other ocean basins. Similarly, in the experiment designated as TANA_{iso} we restore TANA domain SSTs to those of FA while also restoring the TPNP SSTs to CTL values. The TPNP_{iso} and TANA_{iso} experiments allow us to decompose the total effect of basin SST biases (CTL minus experiment) into locally and remotely forced components:

$$\text{CTL} - \text{TPNP} = (\text{CTL} - \text{TPNP}_{\text{iso}}) + (\text{TPNP}_{\text{iso}} - \text{TPNP}) \quad (1)$$

$$\text{CTL} - \text{TANA} = (\text{CTL} - \text{TANA}_{\text{iso}}) + (\text{TANA}_{\text{iso}} - \text{TANA}). \quad (2)$$

The left-hand side represents the total effect and the two terms on the righthand side represent the locally and remotely forced SST effects, respectively.

c. Diagnostic Analyses

208

209 To diagnose the impacts of FLOR’s SST biases on its atmospheric circulation and North
 210 American precipitation, we calculate composite differences between the simulations described
 211 above. To keep the analysis as simple as possible while also illustrating seasonality in the
 212 response, we subdivide the calendar into two six-month seasons, a cold (October – March) and
 213 warm season (April – September). Except for the historical bias calculations, differences express
 214 how CTL compares with the experiment of interest and are calculated as CTL minus the
 215 experiment. To calculate differences in the storm tracks, we identify the storm tracks by the
 216 variance of the high-pass filtered 500 hPa geopotential height (z500) fields, where we use a
 217 Butterworth filter to retain z500 variance with periods less than eight days.

218 To provide further insight into how the circulation and moisture changes induced by SST
 219 biases impact climatological precipitation, we analyze the moisture budget differences between
 220 the experiments. The climatological precipitation budget (e.g. Seager and Henderson 2013) can
 221 be approximated by

$$222 \quad \bar{\bar{P}} = -\frac{1}{\rho_w g} \nabla \cdot \int_0^{p_s} (\bar{\mathbf{u}} \bar{q} + \overline{\mathbf{u}' q'}) dp + \bar{\bar{E}}, \quad (3)$$

223 where P is the precipitation, ρ_w is the density of water, g is the gravitational acceleration, p_s is the
 224 surface pressure, \mathbf{u} is the horizontal wind vector, q is the specific humidity, and E is the surface
 225 evaporation. Double overbars represent climatological seasonal means, and primes represent
 226 deviations from the monthly means, which are at daily resolution in this study. Products of
 227 monthly anomalies are neglected, as the monthly transient eddy convergence term is small over
 228 the domain of interest (not shown). The two terms within the integral represent the effects of
 229 moisture convergence from the climatological flow and the submonthly transient eddy moisture
 230 flux convergence, respectively.

As discussed in Seager and Henderson (2013), the moisture budget calculations are quite sensitive to the horizontal, vertical, and temporal resolution of the archived data, which typically are stored in a standard grid that is distinct from the model's native grid. In the FLOR experiments, the monthly data are saved at 17 standard vertical levels, but the relevant daily data are only available at three vertical levels (surface, 850 hPa, and 500 hPa). The poor vertical resolution of the higher-frequency data means that the transient eddy moisture flux convergence calculations are not reliable. Nevertheless, we evaluated whether the estimates from (3) are accurate enough to provide some insight about the differences in seasonal mean precipitation between the experiments. Figure 4 shows the seasonal CTL minus FA precipitation differences and the corresponding differences estimated by (3). The fields in Fig. 4 are smoothed through 20 iterations of two-dimensional convolution with a 3 x 3 kernel, which especially reduces error in the decomposition by (3) over regions of strongly varying topography. The actual and derived precipitation climatology differences in Fig. 4 agree rather well over the Pacific, North America, and Atlantic regions, indicating that the resolution of the archived data is enough to capture general features in the precipitation budget differences. For the entire Northern Hemisphere, the pattern correlations between the actual precipitation climatology difference pattern and that derived from (1) are 0.89 in October-March and 0.92 in April-September, supporting the reliability of the moisture budget decomposition in capturing the overall spatial differences. The quantitative differences, however, are large enough that caution must be made to avoid overextending the interpretations.

We further subdivide the mean flow convergence component of the precipitation differences into dynamic and thermodynamic components. Specifically, we decompose the climatological precipitation differences between experiments as

$$\delta\bar{P} = -\frac{1}{\rho_w g} \nabla \cdot \int_0^{p_s} ([\delta\bar{\mathbf{u}}]\bar{q} + \bar{\mathbf{u}}[\delta\bar{q}] + \delta\overline{\mathbf{u}'q'}) dp + \delta\bar{E}, \quad (4)$$

where the $[\delta\bar{\mathbf{u}}][\delta\bar{q}]$ term has been neglected because it is much smaller than the other terms. The first term on the right-hand side of (4) represents the impact of the change in climatological circulation, holding the climatological specific humidity constant. We call this term the circulation bias term. The second term on the right-hand side of (4), the humidity bias term, captures the impact of the change in climatological specific humidity, holding the climatological mean flow constant. These two terms indicate whether the removal of SST biases impacts precipitation more strongly through changes in specific humidity that accompany SST changes (thermodynamics) or through impacts of SSTs on the atmospheric circulation, which then impacts precipitation patterns (dynamics).

3. Results

The seasonal North American precipitation biases in the historical FLOR and FLOR-FA simulations, presented as a percentage relative to the observed climatology, are illustrated in Fig. 5. Consistent with Fig. 1, the reduction of SST biases in FLOR-FA reduces or eliminates the precipitation biases over portions of western North America. In the extended winter, flux adjustment reduces precipitation biases over a large portion of North America, although the wet bias persists in FLOR-FA (Fig. 5c). Observational errors in the precipitation climatology, however, are clear in the cold season, as a bias discontinuity is apparent at the United States-Canada border due to differences in precipitation collection technology leading to improved precision in Canada (Adam and Lettenmaier 2003). In the warm season, the bias reduction is even stronger, especially over regions most strongly affected by the NAMS and over the Rockies. This

finding is consistent with recent work that found superior performance of FLOR-FA in simulating the NAMS (Pascale et al. 2017, 2018). We note, however, that FLOR-FA does exacerbate the dry bias over the south-central U.S. in both seasons. Overall, flux adjustment in FLOR reduces the precipitation climatology root-mean-square error over the U.S. region (25-50°N, 60-130°W) by 18.3% in October-March and by 43.4% in April-September. We find nearly identical results when using the other observed precipitation datasets (Figs. S2 and S3).

a. TPNP and TANA simulation results

Next, we analyze the TPNP and TANA simulation results to attribute in a general sense the importance of Pacific and Atlantic SST biases for the FLOR/FLOR-FA climatological precipitation differences. We begin by analyzing climatological differences in precipitation and atmospheric circulation between the 100-yr CTL and each of the TPNP and TANA simulations (designated as δP_{TPNP} and δP_{TANA} for the TPNP and TANA precipitation differences, respectively). A comparison of these plots with the corresponding CTL minus FA plots reveals the degree to which SST biases in the individual basins can explain the differences in the total SST bias-related precipitation differences over North America.

In Fig. 6 we focus on differences in precipitation, sea level pressure (SLP), and 925 hPa wind. The 925 hPa wind corresponds closely with the Caribbean and Great Plains low-level jets, which have a strong impact on the warm season hydroclimate of the central United States (e.g., Krishnamurthy et al. 2015) and are impacted by coupled model SST biases (e.g., Krishnamurthy et al. 2015, 2019). Consistent with the analysis presented earlier, the CTL simulation produces much wetter conditions over southern North America, especially over the southwestern region,

than FA in both the cold and warm seasons (Fig. 6a,b). Figure 6 also reveals that the wetter North America is accompanied by wetter conditions in the equatorial Atlantic and Pacific Oceans, a much deeper wintertime Aleutian low, a weaker summertime North Pacific High and continental low in the North American monsoon region, and a stronger western portion of the summertime North Atlantic Subtropical High (NASH). Fig. 6 presents the precipitation differences as fractional differences relative to the CTL simulation, but the largest absolute differences (shown in Fig. S4) occur in the deep tropics, a region where the differences in convective heating can induce large differences in the extratropical circulation. The cold season composite differences bear a close resemblance to the composites associated with strong El Niño episodes (e.g. Johnson and Kosaka 2016), suggesting a role for tropically forced changes in the large-scale circulation and Pacific storm track, which we explore later. Overall, Figs. 6a and b are consistent with large SST-induced differences in atmospheric circulation that result in stronger imports of atmospheric moisture into southern North America in FLOR relative to FLOR-FA.

The remainder of Fig. 6 illustrates how much of the CTL/FA differences can be explained by tropical and extratropical North Pacific (Fig. 6c,d) or North Atlantic (Fig. 6e,f) differences. The overall impression is that both TPNP and TANA SST biases, primarily negative (Fig. 2), contribute to drier conditions in northern North America and wetter conditions in southern North America. Surprisingly, the TANA SST differences appear to have a dominant influence on the southern North America precipitation and even the North Pacific atmospheric circulation differences in both seasons. In the cold season, both the TANA and TPNP SST biases induce a strengthened Aleutian low, but the Aleutian low response to TANA SST biases is stronger (Fig. 6e). Even more surprisingly, the TANA SST biases induce stronger positive fractional

precipitation biases in the equatorial Pacific Ocean than the direct response to Pacific SST biases, at least in the extended winter season.

We quantify the impacts of North Atlantic and North Pacific SST biases on the climatological CTL/FA precipitation differences in Fig. 7. Specifically, we calculate the percentage of δP_{FA} that can be attributed to δP_{TPNP} and δP_{TANA} . We mask out regions where the CTL/FA precipitation differences are less than 10% of the CTL climatology to focus on regions where the differences are large. The results of Fig. 7 confirm the visual impression of Fig. 6 in that both Atlantic and Pacific SST biases are important for the continental U.S. during the extended winter, that tropical and/or extratropical North Atlantic (North Pacific) SST biases dominate the impacts over southern (northern) North America, and that the Atlantic SST biases are particularly important over the continental U.S. during the extended summer (Fig. 7d). We note, however, that we should not expect the total impact of North Atlantic and North Pacific SST biases to be a linear superposition of the TPNP and TANA simulation results because the Pacific and Atlantic SST biases affect the SST biases in remote ocean basins, as discussed in Section 3c.

The strength of the impact of North Atlantic SST biases on North Pacific precipitation and atmospheric circulation, though surprising, is consistent with recent studies that have examined multi-decadal variability and trends of Atlantic SSTs (Kucharski et al. 2011; McGregor et al. 2014; Li et al. 2016; Ruprich-Robert et al. 2017). In particular, the climate modeling studies of McGregor et al. (2014) and Li et al. (2016) demonstrate that the tropical Atlantic warming trend over the past few decades has the potential to induce negative SST and precipitation trends over the tropical Pacific via modifications of the Walker circulation and coupled ocean/atmosphere feedbacks. These changes in the tropical oceans also impact the circulation and precipitation over the North Pacific and North America (McGregor et al. 2014). Recent studies of Atlantic

multidecadal variability reveal consistent results. Anomalously warm conditions in the tropical Atlantic result in negative precipitation anomalies over the tropical Pacific and an anomalously weak Aleutian low, which impacts the downstream North American climate (Sutton and Hodson 2007; Kushnir et al. 2010; Ruprich-Robert et al. 2017). The negative tropical Atlantic SST biases in FLOR result in the expected response (opposite to that seen from warming) seen in Fig. 6; that is, a stronger Aleutian low.

The results in Fig. 6 generally are consistent with the picture presented above and more generally with the studies of Wang et al. (2007, 2008), which examined the influence of the Atlantic warm pool on Western Hemisphere climate, albeit with a focus only on the summer season. In both the FA and TANA response maps, large negative precipitation differences are present over the tropical Atlantic and northern South America, over and near the regions where tropical Atlantic SST differences are strongly negative. The reduction of atmospheric convection in the Atlantic warm pool results in a “Gill response” (Gill 1980) that manifests as positive SLP differences near and just northwest of the precipitation anomalies (Sutton and Hodson 2007; Wang et al. 2007; Kushnir et al. 2010). The response, however, is not confined to the tropical Atlantic, as the atmospheric Rossby and Kelvin wave response spreads the anomalous cooling to the tropical Pacific, destabilizing the atmosphere and promoting enhanced convection remote from the Atlantic SST forcing (Sutton and Hodson 2007; Kushnir et al. 2010). Therefore, tropical Atlantic cooling promotes a dipole of anomalous convection, with suppressed convection over the tropical western Atlantic and enhanced convection in the central and eastern tropical Pacific.

In boreal winter the enhanced tropical Pacific convection resulting from the Atlantic cooling has the potential to force a Pacific/North American-like (PNA-like) circulation pattern that features an enhanced Aleutian low (Sutton and Hodson 2007; Ruprich-Robert et al. 2017), as

shown in Fig. 6e. The tropical Pacific SST differences also can induce tropical precipitation differences that induce a strengthened Aleutian low (Fig. 6c), but the response is not as strong, possibly because the tropical Pacific SST differences are not as large as the tropical Atlantic SST differences (Fig. 2) and possibly because the tropical Atlantic atmospheric convection anomalies are well positioned to induce remote coupled ocean-atmosphere feedbacks in the tropical Pacific basin (Li et al. 2016; Ruprich-Robert et al. 2017). We examine the remote SST impacts of the Atlantic SST biases in Section 3c.

In the summer months, the Atlantic SST differences potentially can exert stronger direct impacts on North American precipitation (Wang et al. 2007, 2008; Kushnir et al. 2010). Figure 6f indicates positive SLP differences between CTL and TANA over the western tropical Atlantic and over southern North America, which indicate a strengthened western portion of the NASH and a weakened North American monsoon low. This pattern is consistent with the climate model experiments of Wang et al. (2007, 2008) that demonstrated the role of the Atlantic warm pool in modifying the strength of the summertime NASH and the Great Plains and Caribbean low-level jets, which then impacts the northward moisture transport and precipitation in the central U.S. (Wang et al. 2008).

Overall, the results presented in this section suggest both Pacific and Atlantic SST biases prominently drive North American precipitation biases. We also suggest plausible mechanisms that are consistent with previous studies that focused primarily on the impacts of Pacific and Atlantic SST variability. We next examine the roles of tropical and extratropical SST biases, the inter-basin links among the SST biases, and precipitation budget diagnostics to determine if the arguments presented above hold up to further scrutiny.

b. TP and TA simulation results

The arguments regarding the prominent role of Atlantic SST biases on the North Pacific circulation and North American precipitation suggest that tropical rather than extratropical Atlantic SST biases play the more crucial role. The reason is that tropical Atlantic SST biases can directly influence moisture advection into the US, and tropical SST biases can more easily induce upstream circulation impacts due to the larger length scales of the atmospheric response in the tropics relative to the extratropics. To investigate this hypothesis, we show the CTL/TP and CTL/TA seasonal composite differences in circulation and precipitation in Fig. 8. Consistent with expectations, the tropical Atlantic SST biases appear to dominate the Atlantic SST effects on circulation and North American precipitation. In both seasons, the TA results are similar to those of TANA (compare Fig. 8c,d with Fig. 6e,f). The tropical Atlantic precipitation and hemispheric circulation response in the TA results are slightly stronger than that of the TANA experiment, indicating that the extratropical Atlantic SST biases act to damp the full Atlantic SST response slightly, particularly in the extended summer. The reason for this damping requires further investigation, but it appears that colder North Atlantic sea surface in FLOR can induce a stronger NASH that increases moisture convergence in the Caribbean Sea, partially offsetting the reduced moisture and atmospheric instability owing to the colder tropical Atlantic sea surface. The offsetting influence of the extratropical North Atlantic SSTs is consistent with the GCM experiments of Okumura et al. (2009), who investigated the mechanisms by which a large freshwater forcing of the North Atlantic can impact North Pacific climate.

Examination of the TP results suggests that for the Pacific, both tropical and extratropical SST biases contribute to North American precipitation biases in the boreal cold season (compare

Fig. 6c with Fig. 8a) but that tropical SST biases play little role in the boreal warm season. The enhanced subtropical convection in CTL relative to TP in the cold season (Fig. 8a) where CTL SST biases are positive (Fig. 2) may contribute to the slightly stronger Aleutian low through a poleward propagating Rossby wave response. The tropical Pacific SST biases, however, are small relative to the extratropical biases (Fig. 2). The strongly negative SST biases in the central North Pacific in CTL increase the baroclinicity, which also enhances the North Pacific storm track into southern North America. We examine storm track changes more closely in Section 3d. Overall, we find that in the dynamically active boreal cold season, both tropical and extratropical North Pacific SST biases have a substantial impact on FLOR's simulation of North American precipitation. This contrasts the interannual variability of North American precipitation, in which tropical Pacific SSTs are believed to play a much stronger role than extratropical Pacific SST variability (e.g. Kushnir et al. 2002). A key difference is that FLOR's pattern of mean SST biases (with strong biases in the extratropics and in the tropical Atlantic), looks quite different from ENSO SST anomalies, which typically have their strongest signature in the central and eastern equatorial Pacific.

c. TPNP_{iso} and TANA_{iso} simulation results

As discussed above, the SST biases in the North Atlantic and the North Pacific can induce nonlocal SST biases through atmospheric and oceanic pathways. Therefore, the TANA and TPNP simulations do not necessarily isolate the impacts of the SST biases in the basins for which the SSTs have been restored. We illustrate the non-local SST impacts in Fig. 9, which shows the differences in annual mean climatological SSTs between the CTL and each of the TPNP and

TANA simulations. By construction, the SST differences over the North Pacific (North Atlantic) domains defined in Fig. 3 for the TPNP (TANA) simulation are nearly equal to the CTL/FA differences. The SST differences in all other ocean basins are remotely forced.

The SST differences between the CTL and TANA simulation (Fig. 9) reveal that the negative tropical and North Atlantic SST biases induce strongly negative SST biases in the extratropical North Pacific, strongest near 40°N. The North Pacific response to Atlantic SST forcing is consistent with past North Atlantic “water hosing” experiments (Zhang and Delworth 2005; Okumura et al. 2009) in which the North Atlantic is cooled through a large freshwater input as well as recent studies on Atlantic multidecadal variability (Zhang and Delworth 2007; Ruprich-Robert et al. 2017; Johnson et al. 2018) and climate model SST biases (Wang et al. 2014; Zhang and Zhao 2014). Wang et al. (2014) demonstrate that the strength of AMOC may be a key factor in the link between North Pacific and North Atlantic SST biases in the models participating in CMIP5.

Similarly, the tropical and North Pacific SST biases remotely force Atlantic SST biases (Fig. 9a), although the overall impact is not as strong as that of the Atlantic on the Pacific. The negative SST differences over much of the North Atlantic indicate that the removal of the North Pacific SST biases in the TPNP simulation also reduces the negative SST biases in portions of the North Atlantic. In the sub-Arctic North Atlantic, the SST differences are positive, possibly reflecting a shift of the Gulf Stream or changes in the AMOC and oceanic deep convection. Although the amplitude of remote Atlantic SST changes (Fig. 9a) is considerably less than that of the remote Pacific SST changes (Fig. 9b), the North Pacific SST biases induce substantial decreases in the North Atlantic meridional SST gradient (Fig. 9a) and baroclinicity in vicinity of

the North Atlantic storm track, which, as shown in the following section, result in notable increases in evaporation (Figs. 12 and 13) and a reduced storm track intensity (Fig. 15).

To distinguish the roles of local versus remotely forced SST biases, we examine the results of the TANA_{iso} and TPNP_{iso} experiments following the decompositions given in (1) and (2). The decomposition of the Atlantic SST bias effect given by (2) is illustrated in Fig. 10. The top panels show notably stronger precipitation differences over North America than the bottom panels, which indicate a dominance of the locally forced Atlantic SST bias effects. In October – March, the remotely forced effects (Fig. 10c) are consistent with those of the TPNP experiments, indicating that the North Pacific cooling induced by the negative tropical and North Atlantic SST biases induces drying over northern North America and wetting over southern North America. The local and nonlocal Atlantic SST bias effects oppose each other in northern North America but reinforce each other over southern North America (compare Figs. 10a with 10c). In April – September, the local and nonlocal effects oppose each other over most of North America, but the local Atlantic SST effects dominate even more than in the boreal cold season.

The decomposition of the Pacific SST bias effect reveals a more complicated picture (Fig. 11), particularly in the boreal cold season. In October – March over southwestern North America, the local and remote TPNP SST effects reinforce each other, indicating that the negative SST biases in both ocean basins result in increased precipitation. In other parts of North America, the two effects tend to oppose each other. Most conspicuously, the negative TPNP SST bias pattern directly results in positive SLP differences over the North Pacific (Fig. 11a), but the negative SST differences induced in the tropical and North Atlantic (Fig. 9a) force negative SLP differences over the North Pacific (Fig. 11c) that overcompensate the positive SLP differences. This

cancellation between the direct and indirect effect over the North Pacific explains why the impact of the North Pacific SST biases on the North Pacific circulation is relatively modest (Fig. 6c).

The positive SLP response to the negative SST differences over the North Pacific (Fig. 11a) resembles the direct, linear baroclinic response to extratropical SSTs noted in previous studies (Peng et al. 1997; Peng and Whitaker 1999; Kushnir et al. 2002). Specifically, the North Pacific high diminishes in amplitude with height (not shown), consistent with the expected direct response to shallow cooling. However, the total response to extratropical cooling is strongly mediated by synoptic eddies, which is highly sensitive to the background flow (Peng et al. 1997). The total eddy-mediated response to North Pacific cooling in Fig. 11a, with a surface high over the North Pacific and an upper-level trough extending from the eastern Pacific over much of North America (not shown) resembles the response to North Pacific SST anomalies with February background conditions studied in Peng et al. (1997) and Peng and Whitaker (1999). However, those previous studies showed that the response pattern is quite distinct with January background conditions, demonstrating that the synoptic eddy-mediated response to North Pacific extratropical SST anomalies is highly sensitive to the background climatology. Therefore, we urge caution to avoid over generalizing these results.

The remote Pacific SST bias effect over North America is substantial in October – March (Figs. 11c) and generally consistent with the local Atlantic SST bias effect (Fig. 10a). In the context of all other simulation results and previous studies noted above, this finding reinforces that negative tropical Atlantic SST biases in the boreal cold season are effective in inducing an anomalously deep Aleutian low and anomalously wet conditions over much of southern North America. Moreover, a substantial portion of the negative tropical Atlantic SST biases are remotely

forced by the North Pacific SST biases. In the boreal warm season, however, the remotely forced effect of North Pacific SST biases over North America is small (Fig. 11d).

d. Precipitation budget diagnostics

To gain additional insight into the mechanisms that connect SST biases to North American precipitation biases, we examine the contributions to the simulations' climatological precipitation differences determined from equation (4). Specifically, we focus on the circulation bias, humidity bias, and evaporation terms, as these terms generally are the largest contributors to the climatological precipitation differences. As we note above we cannot derive accurate estimates of the contributions by transient eddy convergence owing to insufficient diagnostic output. To shed light on the possible role of differences in transient eddies, we examine differences in the climatological storm tracks.

We first focus on the climatological differences in October – March (Fig. 12). Overall, the circulation bias and evaporation terms make the greatest contributions to the precipitation differences over the North American continent for each pair of experiments. In general, the humidity bias term tends to oppose the changes from the circulation bias term, but the effects of the changing circulation dominate over the thermodynamic effects. Both the TPNP (Fig. 12b) and TANA (Fig. 12c) experiments capture the CTL minus FA circulation bias pattern, with the TANA differences generally showing stronger magnitudes. These findings indicate that the climatological circulation changes induced by the North Pacific and especially tropical Atlantic SST biases dominate the SST-induced differences in wintertime climatological precipitation over North America.

However, there are a number of regions where the circulation bias effects are not the dominant factor during the extended winter season. The CTL minus FA circulation bias pattern (Fig. 12a) features negative differences over Baja California, parts of western North America, and a portion of the southwestern U.S., which contrast the positive precipitation biases in FLOR over this region. These negative circulation-induced differences are overwhelmed by the effects of evaporation (Fig. 12g) and, to a lesser extent, the humidity bias term (Fig. 12d). These opposing influences are captured well in the TPNP experiment (Fig. 12b,e,h). The residual term (bottom row of Fig. 12) generally features positive differences in southern North America and negative differences over the northwest coast of North America. This residual likely reflects, in large part, the omission of the change in transient eddy fluxes from the change in storm tracks, as discussed below.

In contrast with the extended winter, all three terms make sizeable contributions to the climatological precipitation differences from April – September (Fig. 13). Once again, the humidity bias term (second row) tends to oppose the effects of the corresponding circulation term (top row). The combination of the three terms results in a tendency for positive precipitation biases over most of North America (Fig. 4d), but the dominant term varies regionally. Overall, the TANA experiment (right column) captures the total difference patterns (left column) rather well for all three terms, confirming the dominance of the Atlantic SST biases on the SST-related climatological precipitation biases over North America in the FLOR model.

Changes in the storm tracks also modify the transient eddy moisture flux convergence, thereby also contributing to the climatological precipitation differences. Figure 14 provides the climatological storm tracks in CTL, FA, and in reanalysis data for both the extended winter and summer. Compared with CTL (Fig. 14c,f), FA features more northerly displaced North Pacific

and North Atlantic storm tracks in both seasons (Fig. 14b,e), with a somewhat weaker storm track in the western North Pacific in boreal winter. The northward shift of the storm tracks in FA results in improved agreement with the position of the storm tracks derived from reanalysis data (Fig. 14a,b), although the stronger storm track in CTL more closely matches reanalysis data in the western North Pacific region. Overall, Fig. 14 indicates that the SST biases in CTL result in a southward bias in the location of the dominant Northern Hemisphere storm tracks.

The differences in the storm tracks between CTL and FA (Fig. 15a,b) clearly show the southerly displacement over both basins and the stronger North Pacific storm track in CTL. The winter difference pattern resembles, in many respects, the storm track response to El Niño (e.g., Johnson and Kosaka 2016) as well as to the negative phase of the Atlantic Multidecadal Oscillation (Zhang and Delworth 2007), which suggests that SST biases in both the Pacific and Atlantic may contribute to these differences. Consistently, both the TPNP (Fig. 15c,d) and TANA experiments (Fig. 15e,f) produce similar changes to the storm tracks, indicating that both the Atlantic and Pacific SST biases contribute to the stronger and southerly displaced storm tracks in CTL. The storm track differences shown in Fig. 15 closely mirror the differences in 200 hPa zonal wind. The southerly bias in the North Pacific storm track in CTL likely contributes to the wetter conditions in southwestern and drier conditions in northwestern North America relative to FA, a conclusion that is corroborated by the estimated transient eddy contributions to the precipitation budgets, although we choose not to show these results because the insufficient spatial diagnostic outputs limit the reliability of these estimates (Section 2c).

4. Discussion and Conclusions

In this study, we have examined the role of SST biases on the simulation of North American climatological precipitation in a global climate model with 50 km atmospheric horizontal resolution, the GFDL FLOR model. Like many climate models, FLOR simulates excessive precipitation over much of western North America, leading to a failure to simulate the strong east-west contrast in climatological precipitation in observations. A flux-adjusted version of FLOR that greatly reduces SST biases mitigates this deficiency in continental precipitation, indicating that SST biases are a contributor to these precipitation biases. Previous investigations have reached similar conclusions regarding the simulation of the NAMS (Liang et al. 2008; Pascale et al. 2017, 2018), the Great Plains and Caribbean Low-Level Jets (Krishnamurthy et al. 2019), Gulf of California moisture surges into southwestern North America (Pascale et al. 2016), and western United States climatological precipitation in general (Mejia et al. 2018), but the present study focuses on the pathways by which Atlantic and Pacific SST biases contribute to the simulation of excessive precipitation. The main findings of the study are summarized in schematic diagrams shown in Fig. 16. Because the SST biases in FLOR share many features common to many or even most current global climate models (e.g., Wang et al. 2014; Richter 2015), the results presented here likely apply broadly to a range of climate models.

From the analysis presented here, a few general themes emerge. First, relative to the Pacific, FLOR's Atlantic SST biases make a substantially greater contribution to the excessive precipitation in the western U.S. and Mexico for both seasons. One reason appears to be substantially stronger SST biases in the tropical Atlantic relative to the tropical Pacific in FLOR, given that tropical SST biases are most effective in exciting large-scale circulation responses owing to their effects on tropical convection and Rossby wave sources. Although the relative strength of the tropical Pacific SST biases may differ in other climate models, the strong tropical

Atlantic SST biases are pervasive in the current generation of global climate models (Li and Xie 2014; Wang et al. 2014). Another factor is the effectiveness of tropical Atlantic SST biases to induce substantial circulation and moisture anomalies both locally, through changes in the NASH and associated low-level jets, and nonlocally in the Indian and Pacific Oceans, through modifications of the Walker circulation. The latter mechanism, which has been corroborated in several recent studies on Atlantic multidecadal variability, results in a strong link between negative SST biases in the tropical Atlantic and an anomalously deepened Aleutian low and an associated southerly shift of the storm tracks, which contribute substantially to the wet bias over western North America. Overall, these findings suggest that reductions of tropical Atlantic SST biases in coupled GCMs, which appear to be closely tied to biases in the Atlantic meridional overturning circulation (Wang et al. 2014), would have substantial benefits for the simulation of precipitation over the United States and Central America, especially in boreal summer.

Another emerging theme is the difficulty in isolating the effects of local SST biases owing to precipitation responses to remote SST effects, e.g., the response of precipitation to the SST changes induced in the North Pacific by Atlantic SST biases. Negative SST biases in the Atlantic induce negative SST biases in the extratropical Pacific, and negative SST biases in the North Pacific induce negative SST biases in both the tropical and extratropical North Atlantic. Both the local and remotely forced SST biases appear to have substantial influences on the atmospheric circulation and North American precipitation. Another apparently important factor for the reduced impact of the North Pacific SST biases relative to North Atlantic SST biases is the competing impacts of the local North Pacific and remotely forced SST bias impacts on the North Pacific atmospheric circulation. Specifically, the North Pacific surface high forced by local negative SST biases partially offsets the deepened Aleutian low response to the remotely forced negative tropical

Atlantic SST biases (Fig. 11a,c). However, these competing effects may be challenging to disentangle in studies with multi-model ensembles, as previous studies have demonstrated that the eddy-mediated response to extratropical SST forcing is sensitive to the details of the background flow.

As discussed in Section 1, various processes and modeling deficiencies contribute to the pervasive SST biases in the current generation of global climate models. As both parameterizations improve and model resolution increases, we expect that these SST biases accordingly shall reduce. The findings presented here provide insight into the expected changes in climatological precipitation over North America as these SST biases are reduced, regardless of whether the precipitation biases in other models are stronger or weaker than those of FLOR. This study also suggests that flux adjustment may remain a viable intermediate solution for problems for which climatological precipitation simulation is critical. For example, the improved simulation of the North American monsoon in FLOR-FA has enabled new insights into projected changes of this monsoon system under global warming (Pascale et al. 2017, 2018). These recent studies illuminate how the climate sensitivity of some facets of the climate system may be affected by climatological SST biases and how the removal of these biases through flux adjustment can improve confidence in projected changes. In addition, a set of seasonal hindcasts with FLOR-FA successfully captured the western U.S. precipitation pattern during the El Niño winter of 2015-16, a pattern that was generally poorly predicted and atypical of other strong El Niño events (Yang et al. 2018). This finding raises questions about how the reduction of SST biases may impact seasonal forecasts of western U.S. precipitation. Future work shall address how SST biases may impact other aspects of the variability, prediction skill, and projected changes of North American precipitation, including the tails of precipitation distribution.

Acknowledgments.

We thank three anonymous reviewers for constructive comments that greatly benefited this manuscript. We also thank Drs. Liping Zhang and Xiaosong Yang for helpful comments on an earlier version of the manuscript. N. C. Johnson, L. Krishnamurthy, and S. Pascale were supported by awards NA14OAR4320106 and NA18OAR4320123 from the National Oceanic and Atmospheric Administration, U.S. Department of Commerce. NCEP/NCAR Reanalysis and precipitation data are provided by the NOAA/OAR/ESRL PSD, Boulder, Colorado, USA, from their Web site at <http://www.esrl.noaa.gov/psd/>.

References

- Adam, J.C. and D. P. Lettenmaier, 2003: Adjustment of global gridded precipitation for systematic bias. *JGR:Atmospheres*, 108(D9), doi:[10.1029/2002JD002499](https://doi.org/10.1029/2002JD002499).
- Adcroft, A. J., and Co-authors, 2019: The GFDL global ocean and sea ice model OM4.0: Model description and simulation features. *J. Adv. Model. Earth Syst.*, doi:10.1029/2019MS001726.
- Balaji, V., I. Held, M. Winton, S. Malyshev, and R. Stouffer, 2006: The Exchange Grid: A mechanism for data exchange between Earth System components on independent grids. *Parallel Computational Fluid Dynamics: Theory and Applications: Proceedings of the 2005 International Conference on Parallel Computational Fluid Dynamics*, A. Deane et al., Eds., Elsevier, 33–41.

Chen, M., P. Xie, J. E. Janowiak, and P. A. Arkin, 2002: Global Land Precipitation: A 50-yr
Monthly Analysis Based on Gauge Observations, *J. Hydrometeorology*, 3, 249-266.

Dai, A., 2006: Precipitation characteristics in eighteen coupled climate models. *J. Climate*, **19**,
4605-4630.

Dai, A., and K. E. Trenberth, 2004: The diurnal cycle and its depiction in the Community Climate
System Model. *J. Climate*, **17**, 930-951.

Delworth, T. L., and Coauthors, 2012: Simulated climate and climate change in the GFDL CM2.5
high-resolution coupled climate model. *J. Climate*, 25, 2755-2781, doi:10.1175/JCLI-D-11-
00316.1.

Geil, K. L., Y. L. Serra, and X. Zeng, 2013: Assessment of CMIP5 Model Simulations of the North
American Monsoon System. *J. Climate*, **26**, 8787-8801.

Gill, A. E., 1980: Some simple solutions for heat-induced tropical circulation. *Quart. J. Roy.
Meteor. Soc.*, **106**, 447-462.

Griffies, S. M., and Co-authors, 2015: Impacts on ocean heat from transient mesoscale eddies in a
hierarchy of climate models. *J. Climate*, **28**, 952-977, doi: 10.1175/JCLI-D-14-00353.1.

685 Held, I. M., and Co-authors, 2019: Structure and performance of GFDL's CM4.0 climate model.
686 *J. Adv. Model. Earth Syst.*, in press, doi:10.1029/2019MS001829.
687

688 Jia, L., and Co-authors, 2015: Improved seasonal prediction of temperature and precipitation over
689 land in a high-resolution GFDL climate model. *J. Climate*, **28**, 2044-2062, doi:10.1175/JCLI-D-
690 14-00112.1.
691

692 Jia, L., G. A. Vecchi, X. Yang, R. G. Gudgel, T. L. Delworth, W. F. Stern, K. Paffendorf, S. D.
693 Underwood, and F. Zeng, 2016: The roles of radiative forcing, sea surface temperatures, and
694 atmospheric and land initial conditions in U.S. summer warming episodes. *J. Climate*, **29**, 4121-
695 4135, doi:10.1175/JCLI-D-15-0471.1.
696

697 Jiang, X., B. Xiang, M. Zhao, T. Li, S.-J. Lin, Z. Wang, and J.-H. Chen, 2018: Intraseasonal
698 Tropical Cyclogenesis Prediction in a Global Coupled Model System. *J. Climate*, **31**, 6209-6227,
699 doi:[10.1175/JCLI-D-17-0454.1](https://doi.org/10.1175/JCLI-D-17-0454.1).
700

701 Johnson, N. C., and Y. Kosaka, 2016: The impact of eastern equatorial Pacific convection on the
702 diversity of boreal winter El Niño teleconnection patterns. *Climate Dyn.*, **47**, 3737-3764,
703 doi:10.1007/s00382-016-3039-1.
704

705 Johnson, N. C., S.-P. Xie, Y. Kosaka, and X. Li, 2018: Increasing occurrence of cold and warm
706 extremes during the recent global warming slowdown. *Nature Communications*, **9**, 1724,
707 doi:10.1038/s41467-018-04040-y.

708

709 Kalnay E., and Co-authors, 1996: The NCEP/NCAR 40-Year Reanalysis Project. *Bull. Amer.*
710 *Meteor. Soc.*, **77**, 437-471.

711

712 Kapnick, S. B. X. Yang, G. A. Vecchi, T. L. Delworth, R. Gudgel, S. Malyshev, P. C. D. Milly,
713 E. Shevliakova, S. Underwood, and S. A. Margulis, 2018: Potential for western US seasonal
714 snowpack prediction. *Proc. Nat. Acad. Sci.*, **115**, 1180-1185, doi:10.1073/pnas.1716760115.

715

716 Keeley, S. P. E., R. T. Sutton, and L. C. Shaffrey, 2012: The impact of North Atlantic sea surface
717 temperature errors on the simulation of North Atlantic European region climate. *Q. J. Roy. Met.*
718 *Soc.*, **138**, 1774-1783.

719

720 Kirtman, B. P., and Co-authors, 2012: Impact of ocean model resolution on CCSM climate
721 simulations. *Clim. Dyn.*, **39**, 1303-1328, doi:10.1007/s00382-012-1500-3.

722

723 Krishnamurthy, L., A. G. Muñoz, G. A. Vecchi, R. Msadek, A. T. Wittenberg, B. Stern, R. Gudgel,
724 and F. Zeng, 2019: Assessment of summer rainfall forecast skill in the Intra-Americas in GFDL
725 high and low-resolution models. *Climate Dyn.*, **52**, 1965-1982, doi: 10.1007/s00382-018-4234-z.

726

727 Krishnamurthy, L., G. A. Vecchi, R. Msadek, A. Wittenberg, T. L. Delworth, and F. Zeng, 2015:
728 The seasonality of the Great Plains low-level jet and ENSO relationship. *J. Climate*, **28**, 4525-
729 4544, doi:10.1175/JCLI-D-14-00590.1.

730

Kucharski, F., I.-S. Kang, R. Farneti, and L. Feudale, 2011: Tropical Pacific response to 20th century Atlantic warming. *Geophys. Res. Lett.*, **38**, L03702, doi:10.1029/2010GL046248.

Kushnir, Y., W. A. Robinson, I. Bladé, N. M. J. Hall, S. Peng, R. Sutton, 2002: Atmospheric GCM response to extratropical SST anomalies: Synthesis and evaluation. *J. Climate*, **15**, 2233-2256.

Kushnir, Y., R. Seager, M. Ting, N. Naik, and J. Nakamura, 2010: Mechanisms of tropical Atlantic SST influence on North American precipitation variability. *J. Climate*, **23**, 5610-5628, doi:10.1175/2010JCLI3172.1.

Large, W. G., and G. Danabasoglu, 2006: Attribution and impacts of upper-ocean biases in CCSM3. *J. Climate*, **19**, 2325-2346.

Li, G., and S.-P. Xie, 2014: Tropical biases in CMIP5 multimodel ensemble: The excessive equatorial Pacific cold tongue and double ITCZ problems. *J. Climate*, **27**, 1765-1780.

Li, X., S.-P. Xie, S. T. Gille, and C. Yoo, 2016: Atlantic-induced pan-tropical climate change over the past three decades. *Nature Clim. Change*, **6**, 275-279, doi:10.1038/nclimate2840.

Liang, X.-Z., J. Zhu, K. E. Kunkel, M. Ting, and J. X. L. Wang, 2008: Do CGCMs simulate the North American monsoon precipitation seasonal-interannual variability? *J. Climate*, **21**, 4424-4448.

754 Lin, J.-L., 2007: The double-ITCZ problem in IPCC AR4 coupled GFCMs: Ocean-atmosphere
755 feedback analysis. *J. Climate*, **20**, 4497-4525.

756

757 Liu, Z., A. Mehran, T. J. Phillips, and A. AghaKouchak, 2014: Seasonal and regional biases in
758 CMIP5 precipitation simulations. *Clim. Res.*, **60**, 35-40, doi: 10.3354/cr01221.

759

760 McGregor, S., A. Timmermann, M. F. Stuecker, M. H. England, M. Merrifield, F.-F. Jin, and Y.
761 Chikamoto, 2014: Recent Walker circulation strengthening and Pacific cooling amplified by
762 Atlantic warming. *Nature. Clim. Change*, **4**, 888-892, doi:10.1038/nclimate2330.

763

764 Mechoso, C., and Coauthors, 1995: The seasonal cycle over the tropical Pacific in coupled ocean-
765 atmosphere general circulation models. *Mon Wea. Rev.*, **123**, 2825-2838.

766

767 Mehran, A., A. AghaKouchak, and T. J. Phillips, 2014: Evaluation of CMIP5 continental
768 precipitation simulations relative to satellite-based gauge-adjusted observations. *J. Geophys. Res.*,
769 **119**, 1695-1707, doi:10.1002/2013JD021152.

770

771 Mejia, J. F., D. Koraćin, and E. M. Wilcox, 2018: Effect of coupled global climate models sea
772 surface temperature biases on simulated climate of the western United States. *Int. J. Climatol.*, **38**,
773 5386-5404, doi:10.1002/joc.5817.

774

Murakami, H., G. Villarini, G. A. Vecchi, W. Zhang, and R. Gudgel, 2016: Statistical-dynamical seasonal forecast of North Atlantic and U.S. landfalling tropical cyclones using the high-resolution GFDL FLOR coupled model. *Mon. Wea. Rev.* **144**, 2101-2123, doi:10.1175/MWR-D-15-0308.1.

Okumura, Y. M., C. Deser, A. Hu, A. Timmermann, and S.-P. Xie, 2009: North Pacific climate response to freshwater forcing in the subarctic North Atlantic: Oceanic and atmospheric pathways. *J. Climate*, **22**, 1424-1445, doi:10.1175/2008JCLI2511.1.

Pascale, S., W. R. Boos, S. Bordoni, T. L. Delworth, S. B. Kapnick, H. Murakami, G. A. Vecchi, and W. Zhang, 2017: Weakening of the North American monsoon with global warming. *Nature Clim. Change*, **7**, 806-812, doi:10.1038/nclimate3412.

Pascale, S., S. Bordoni, S. B. Kapnick, G. A. Vecchi, T. L. Delworth, S. Underwood, and W. Anderson, 2016: The impact of horizontal resolution on North American monsoon Gulf of California moisture surges in a suite of coupled global climate models. *J. Climate*, **29**, 7911-7936.

Pascale, S., S. B. Kapnick, S. Bordoni, and T. L. Delworth, 2018: The influence of CO₂ forcing on North American Monsoon moisture surges. *J. Climate*, **31**, 7949-7968.

Pascale, S., V. Lucarini, X. Feng, A. Porporato, and S. ul Hasson, 2015: Analysis of rainfall seasonality from observations and climate models. *Climate Dyn.*, **44**, 3281-3301, doi:10.1007/s00382-014-2278-2.

Peng, S., W. A. Robinson, and M. P. Hoerling, 1997: The modeled atmospheric response to midlatitude SST anomalies and its dependence on background circulation states. *J. Climate*, **10**, 971-987.

Peng, S. and J. S. Whitaker, 1999: Mechanisms determining the atmospheric response to midlatitude SST anomalies. *J. Climate*, **12**, 1393-1408.

Phillips, T. J. and P. J. Gleckler, 2006: Evaluation of continental precipitation in 20th century climate simulations: The utility of multimodel statistics. *Water Resources Res.*, **42**, W03202, doi:10.1029/2005WR004313.

Rayner, N. A., D. E. Parker, E. B. Horton, C. K. Folland, L. V. Alexander, D. P. Rowell, E. C. Kent, and A. Kaplan, 2003: Global analyses of sea surface temperature, sea ice, and night marine air temperature since the late nineteenth century. *J. Geophys. Res.*, **108**, 4407, doi:10.1029/2002JD002670.

Richter, I., 2015: Climate model biases in the eastern tropical oceans: causes, impacts, and ways forward. *WIREs Clim. Change*, **6**, 345-358.

Ruprich-Robert, Y., R. Msadek, F. Castruccio, T. Delworth, and G. Danabasoglu, 2017: Assessing the climate impacts of the observed Atlantic Multidecadal Variability using GFDL CM2.1 and NCAR CESM1 global coupled models. *J. Climate*, in press, doi:10.1175/JCLI-D-16-0127.1

Schneider, U., A. Becker, P. Finger, A. Meyer-Christoffer, M. Ziese, and B. Rudolf, 2014: GPCC's new land surface precipitation climatology based on quality-controlled in situ data and its role in quantifying the global water cycle. *Theor. Appl. Climatol.*, **115**, 15–40, doi:<https://doi.org/10.1007/s00704-013-0860-x>.

Seager, R., and N. Henderson, 2013: Diagnostic computation of moisture budgets in the ERA-Interim Reanalysis with reference to analysis of CMIP-archived atmospheric model data. *J. Climate*, **26**, 7876-7901, doi:10.1175/JCLI-D-13-00018.1.

Stephens, G. L., T. L'Ecuyer, R. Forbes, A. Gettleman, J.-C. Golaz, A. Bodas-Salcedo, K. Suzuki, P. Gabriel, and J. Haynes, 2010: Dreary state of precipitation in global models. *J. Geophys. Res.*, **115**, D24211, doi:10.1029/2010JD014532.

Sheffield J., and Co-authors, 2013: North American climate in CMIP5 experiments. Part I: Evaluation of historical simulations of continental and regional climatology. *J. Climate*, **26**, 9209-9245.

Sutton, R. T., and D. L. R. Hodson, 2007: Climate response to basin-scale warming and cooling of the North Atlantic Ocean. *J. Climate*, **20**, 891-907.

Sun, Y., S. Solomon, A. Dai, and R. W. Portmann, 2006: How often does it rain? *J. Climate*, **19**, 916-934.

Trenberth, K. E., A. Dai, R. M. Rasmussen, and D. B. Parsons, 2003: The changing character of precipitation. *Bull. Amer. Meteor. Soc.*, **84**, 1205-1217.

Van der Wiel, K., S. B. Kapnick, G. A. Vecchi, W. F. Cooke, T. L. Delworth, L. Jia, H. Murakami, S. Underwood, and F. Zeng. (2016): "The Resolution Dependence of Contiguous U.S. Precipitation Extremes in Response to CO₂ forcing." *Journal of Climate* 29 (22): 7991-8012. doi:10.1175/JCLI-D-16-0307.1

Vecchi, G. A., and Co-authors., 2014: On the seasonal forecasting of regional tropical cyclone activity. *J. Climate*, **27**, 7994-8016.

Vecchi, G. A., and Co-authors, 2019: Tropical cyclone sensitivities to CO₂ doubling: Roles of atmospheric resolution, synoptic variability and background climate changes. *Climate Dyn.*, **53**, 5999-6033, doi:10.1007/s00382-019-04913-y.

Wang, C., S.-K. Lee, and D. B. Enfield, 2007: Impact of the Atlantic warm pool on summer climate of the Western Hemisphere. *J. Climate*, **20**, 5021-5040, doi:10.1175/JCLI4304.1.

Wang, C., S.-K. Lee, and D. B. Enfield, 2008: Climate response to anomalously large and small Atlantic warm pools during the summer. *J. Climate*, **21**, 2437-2450, doi:10.1175/JCLI2029.1.

Wang, C., L. Zhang, S.-K. Lee, L. Wu, and C. R. Mechoso, 2014: A global perspective on CMIP5 climate model biases. *Nature. Clim. Change*, **4**, 201-205.

867

868 Wilcox, E. M. and L. J. Donner, 2007: The frequency of extreme rain events in satellite rain-rate
869 estimates and an atmospheric General Circulation Model. *J. Climate*, **20**, 53-69.

870

871 Willmott, C. J., and K. Matsuura, 2001: Terrestrial air temperature and precipitation: Monthly and
872 annual time series (1950 - 1999),
873 http://climate.geog.udel.edu/~climate/html_pages/README.ghcn_ts2.html.

874

875 Wittenberg, A. T., G. A. Vecchi, T. L. Delworth, A. Rosati, W. Anderson, W. F. Cooke, S.
876 Underwood, F. Zeng, S. Griffies, and S. Ray, 2018: Improved simulations of tropical Pacific
877 annual-mean climate in the GFDL FLOR and HiFLOR coupled GCMs. *J. Adv. Model. Earth Syst.*,
878 **10**, 3176-3220, doi:10.1029/2018MS001372.

879

880 Xiang, B., S.-J. Lin, M. Zhao, N. C. Johnson, X. Yang, and X. Jiang, 2019: Subseasonal Week 3–
881 5 Surface Air Temperature Prediction During Boreal Wintertime in a GFDL Model. *Geophys. Res.*
882 *Lett.*, **46**, 416-425, doi:[10.1029/2018GL081314](https://doi.org/10.1029/2018GL081314).

883

884 Xiang, B., S.-J. Lin, M. Zhao, S. Zhang, G. Vecchi, T. Li, X. Jiang, L. Harris, and J.-H. Chen,
885 2014: Beyond Weather Time-Scale Prediction for Hurricane Sandy and Super Typhoon Haiyan in
886 a Global Climate Model. *Mon. Weather Rev.*, **143**, 524-535.

887

888 Xu, Z., P. Chang, I. Richter, W. Kim, and G. Tang, 2014: Diagnosing southeast tropical Atlantic
889 SST and ocean circulation biases in the CMIP5 ensemble. *Clim. Dyn.*, **43**, 3123-3145,
890 doi:10.1007/s00382-014-2247-9.

891

892 Yang, X., and Coauthors, 2015: Seasonal predictability of extratropical storm tracks in GFDL's
893 high-resolution climate prediction model. *J. Climate*, **28**, 3592-3611, doi:10.1175/JCLI-D-14-
894 00517.1.

895

896 Yang, Z., and Coauthors, 2018: On the seasonal prediction of the western United States El Niño
897 precipitation pattern during the 2015/16 winter. In Press at *Clim. Dyn.*, doi:10.1007/s00382-018-
898 4109-3.

899

900 Zhang, L., C. Wang, Z. Song, and S.-K. Lee, 2014: Remote effect of the model cold bias in the
901 tropical North Atlantic on the warm bias in the tropical southeastern Pacific. *J. Adv. Model. Earth*
902 *Sys.*, **6**, 1016-1026, doi:10.1002/2014MS000338.

903

904 Zhang, L., and C. Zhao, 2014: Processes and mechanisms for the model SST biases in the North
905 Atlantic and North Pacific: A link with the Atlantic meridional overturning circulation. *J. Adv.*
906 *Model. Earth Syst.*, **7**, 739-758, doi:10.1002/2014MS000415.

907

908 Zhang, R., and T. L. Delworth, 2005: Simulated tropical response to a substantial weakening of
909 the Atlantic thermohaline circulation. *J. Climate*, **18**, 1853-1860, doi:10.1175/JCLI3460.1.

Zhang, R., and T. L. Delworth, 2007: Impact of the Atlantic Multidecadal Oscillation on the North Pacific climate variability. *Geophys. Res. Lett.*, **34**, L23708, doi:10.1029/2007GL031601.

Zuidema, P. and Co-authors, 2016: Challenges and prospects for reducing coupled climate model SST biases in the eastern tropical Atlantic and Pacific Oceans: The U.S. CLIVAR Eastern Tropical Oceans Synthesis Working Group.. *Bull. Amer. Meteor. Soc.*, **97**, 2305–2328, <https://doi.org/10.1175/BAMS-D-15-00274.1>.

List of Figures

FIG. 1. Climatological (1951-2010) annual precipitation (mm d^{-1}) in (a) observations, (b) FLOR, and (c) FLOR-FA.

FIG. 2. Climatological (1951-2010) annual SST biases (K) in (a) FLOR and (b) FLOR-FA.

FIG. 3. Regions for which SSTs are restored to FA values (dark red) in (a) TPNP, (b) TANA, (c) TP, and (d) TA experiments. The regions in which the color smoothly transitions from red to blue indicate the buffer regions where the restoring is relaxed to zero.

FIG. 4. CTL minus FA climatological precipitation differences (mm d^{-1}) for (a,c) October – March and (b,d) April – September. The top panels are the actual differences and bottom panels are derived from the budget decomposition estimated from (1).

FIG. 5. Climatological precipitation biases (% relative to U. Delaware precipitation) over North America in (top) FLOR and (bottom) FLOR-FA for (a,c) October – March and (b,d) April – September. The values in the lower right corner of each panel are the RMSE (mm d^{-1}) in the U.S. region (red box in a).

FIG. 6. FIG. 6. Impact of (left) October – March and (right) April – September (top) global, (middle) tropical and extratropical Pacific, and (bottom) tropical and extratropical Atlantic FLOR SST biases, including the effects of remotely induced SST biases, as expressed by the (a,b) CTL minus FA, (c,d) CTL minus TPNP, and (e,f) CTL minus TANA climatological differences in precipitation (color shading), SLP (contours), and 925 hPa wind (vectors) for (left) October – March and (right) April – September. Precipitation differences are expressed as percentage relative to CTL climatology. SLP is contoured at intervals of 1 hPa with red (blue) lines indicating positive (negative) differences, and the zero contour is omitted. The reference vector for 925 hPa wind is shown in the bottom right of panel d.

FIG. 7. Percent of $\delta P_{\text{FLOR-FA}}$ that can be attributed to (a,b) TPNP and (c,d) TANA domain SST differences for (left) October – March and (right) April – September. Areas masked in grey represent regions where the FLOR-CTL minus FLOR-FA precipitation differences are less than 10% of the FLOR-CTL climatological precipitation.

FIG. 8. Impact of (top) tropical Pacific and (bottom) tropical Atlantic FLOR SST biases, including the effects of remotely induced SST biases, as expressed by the (a,b) CTL minus TP and (c,d) CTL minus TA climatological differences in precipitation (color shading), SLP (contours), and 925 hPa

wind (vectors) for (left) October – March and (right) April – September. Precipitation differences are expressed as percentage relative to CTL climatology. SLP is contoured at intervals of 1 hPa with red (blue) lines indicating positive (negative) differences, and the zero contour is omitted. The reference vector for 925 hPa wind is shown in the bottom right of panel b.

FIG. 9. (a) CTL minus TPNA and (b) CTL minus TANA annual mean climatological SST differences (K).

FIG. 10. As in Fig. 8 except for the (a,b) locally forced tropical and extratropical North Atlantic SST effect (CTL minus $TANA_{iso}$) and the (c,d) remotely forced tropical and extratropical North Atlantic SST effect ($TANA_{iso}$ minus TANA).

FIG. 11. As in Fig. 8 except for the (a,b) locally forced tropical and extratropical North Pacific SST effect (CTL minus $TPNP_{iso}$) and the (c,d) remotely forced tropical and extratropical North Pacific SST effect ($TPNP_{iso}$ minus TPNP).

FIG. 12. Contributions to the October – March (left column) CTL minus FA, (middle column) CTL minus TPNP, and (right column) CTL minus TANA climatological precipitation differences ($mm\ d^{-1}$) attributed to the following terms: (a-c) circulation bias, (d-f) humidity bias, (g-i) evaporation, and (j-l) the residual, calculated as the actual precipitation difference minus the sum of the three terms.

FIG. 13. As in Fig. 12 but for April – September.

979

980 FIG. 14. Climatological storm tracks, as measured by 8-day high-pass filtered 500 hPa geopotential
981 height variance (shading, m^2) and 200 hPa zonal wind (grey contours at an interval of 10 ms^{-1}) for
982 (left) NCEP/NCAR reanalysis data, (center) FA, and (right) CTL simulations in (a-c) October –
983 March and (d-f) April – September.

984

985 FIG. 15. Differences in climatological storm tracks, as measured by 8-day high-pass filtered 500
986 hPa geopotential height variance (shading, m^2), and 200 hPa zonal wind (grey contours at an
987 interval of 2 ms^{-1} , zero contour is omitted) for (a,b) CTL minus FA, (c,d) CTL minus TPNP, and
988 (e,f) CTL minus TANA in (left) October – March and (right) April – September.

989

990 FIG. 16. Schematic showing the dominant impacts of Pacific and Atlantic SST biases on North
991 American precipitation biases in the boreal cold and warm seasons. In the boreal cold season, (a)
992 negative SST biases in the extratropical North Pacific promote a strengthened and southerly shifted
993 storm track, which enhances precipitation in the southwestern United States and suppresses
994 precipitation in northern Canada. (b) Tropical Atlantic cold SST biases induce circulation changes
995 throughout the entire tropics resembling the classic Gill model, with a surface anticyclone in the
996 vicinity of the cold bias and low-level convergence and enhanced precipitation in the equatorial
997 Pacific. The enhanced tropical Pacific rainfall excites a deepened Aleutian low and enhanced
998 moisture transport and precipitation in the southern United States. In the boreal warm season, the
999 effects of (c) North Pacific SST biases are modest, but a weaker northern portion of the North
1000 Pacific storm track promotes drier conditions in northern North America. (d) The cold Atlantic
1001 SST biases have a much stronger impact, substantially strengthening the western lobe of the North

1002 Atlantic Subtropical High and weakening the thermal low over southern North America. These
1003 changes enhance the Great Plains Low Level jet and moisture transport into southwestern North
1004 America. Because the SST biases in each basin influence the SST biases in the other basin, the
1005 total SST bias effects are not limited to the direct effects described here.

1006

1007

1008

1009

1010

1011

1012

1013

1014

1015

1016

1017

1018

1019

1020

1021

1022

1023

1024

1025 Table 1. List of FLOR experiments analyzed in this study.

| Experiment name | Description | Duration (years) |
|---------------------|---|------------------|
| CTL | FLOR with 1990 radiative forcings | 100 |
| FA | FLOR with 1990 radiative forcings and flux adjustments to correct SST biases | 100 |
| TPNP | CTL but with tropical and extratropical North Pacific SSTs restored to FA values | 100 |
| TANA | CTL but with tropical and extratropical North Atlantic SSTs restored to FA values | 100 |
| TP | CTL but with tropical Pacific SSTs restored to FA values | 100 |
| TA | CTL but with tropical Atlantic SSTs restored to FA values | 100 |
| TPNP _{iso} | As in TPNP but with tropical and extratropical North Atlantic SSTs restored to CTL values | 50 |
| TANA _{iso} | As in TANA but with tropical and extratropical North Pacific SSTs restored to CTL values | 50 |

1026

1027

1028

1029

1030

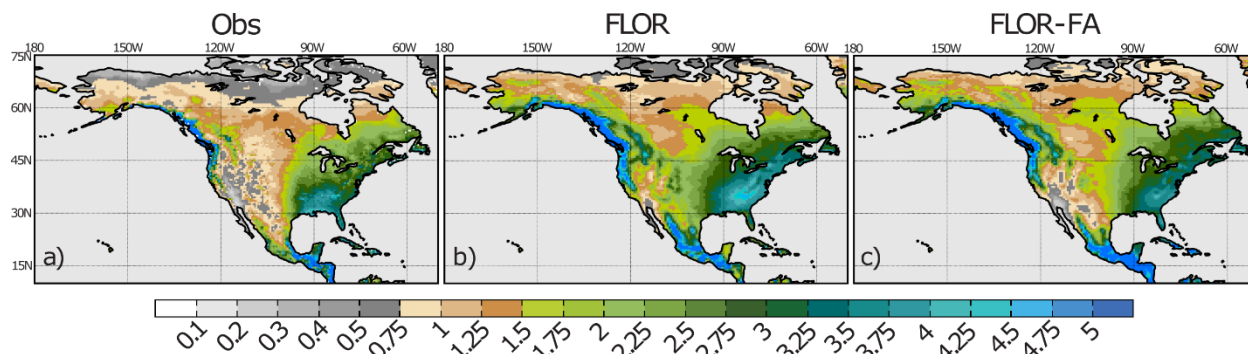


FIG. 1. Climatological (1951-2010) annual precipitation (mm d⁻¹) in (a) observations, (b) FLOR, and (c) FLOR-FA.

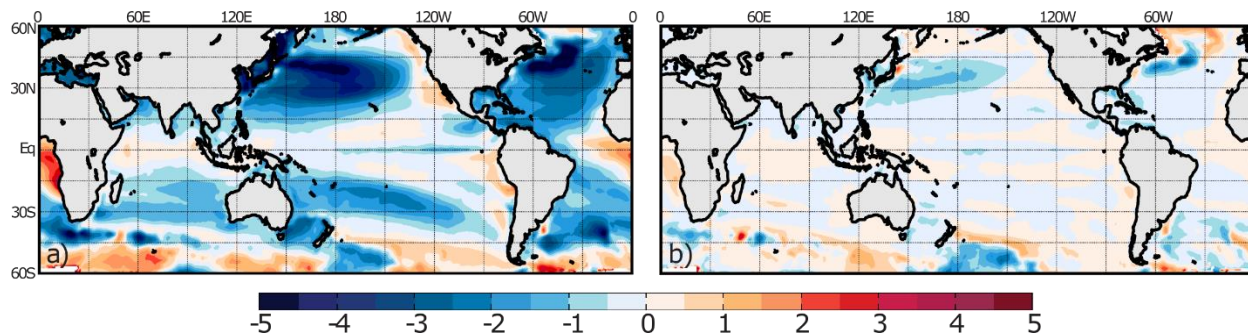


FIG. 2. Climatological (1951-2010) annual SST biases (K) in (a) FLOR and (b) FLOR-FA.

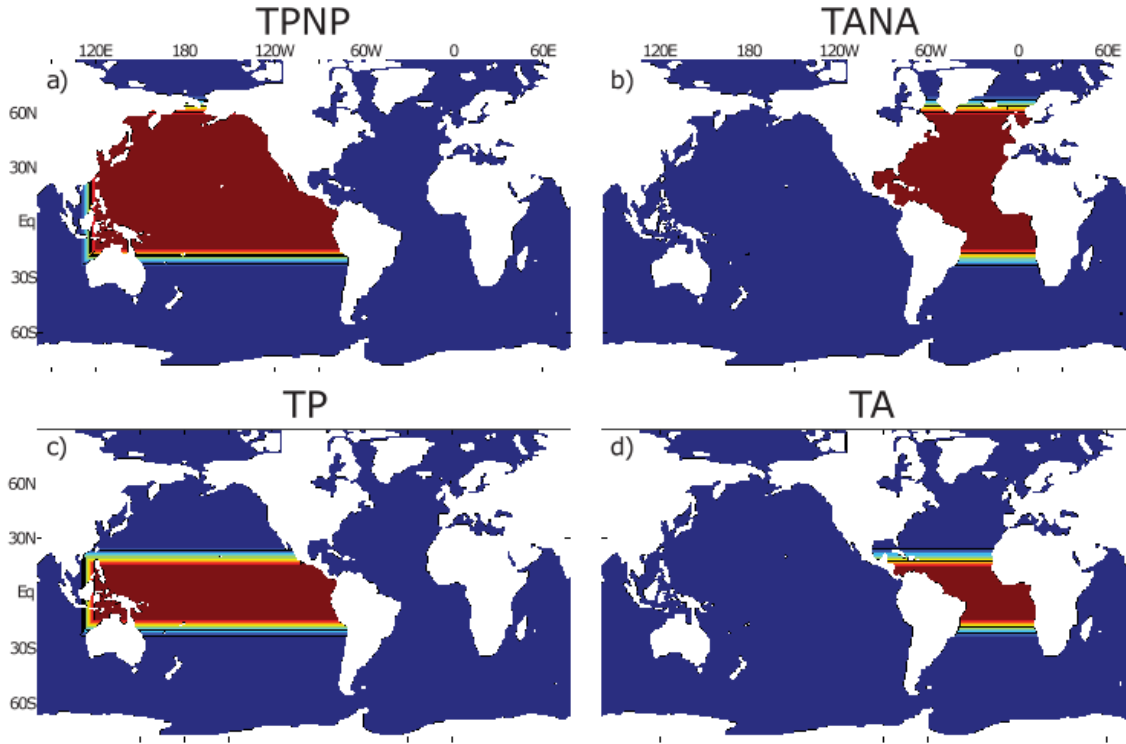


FIG. 3. Regions for which SSTs are restored to FA values (dark red) in (a) TPNP, (b) TANA, (c) TP, and (d) TA experiments. The regions in which the color smoothly transitions from red to blue indicate the buffer regions where the restoring is relaxed to zero.

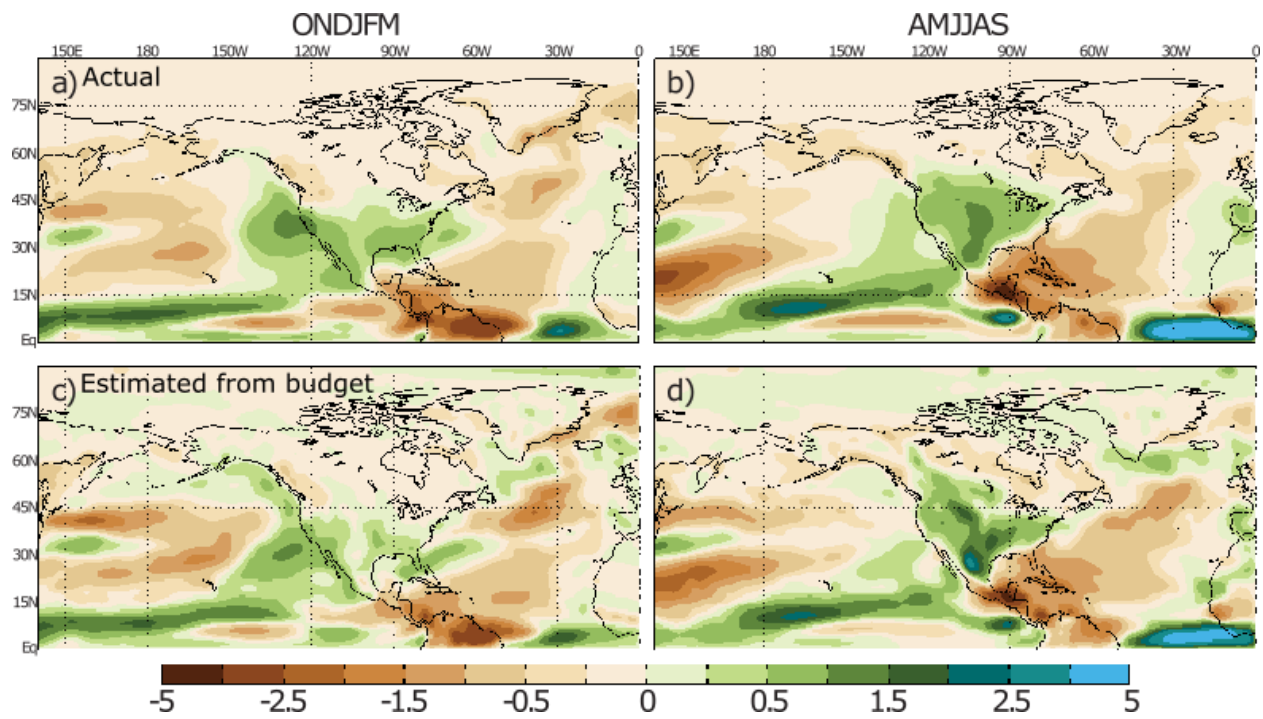


FIG. 4. CTL minus FA climatological precipitation differences (mm d⁻¹) for (a,c) October – March and (b,d) April – September. The top panels are the actual differences and bottom panels are derived from the budget decomposition estimated from (1).

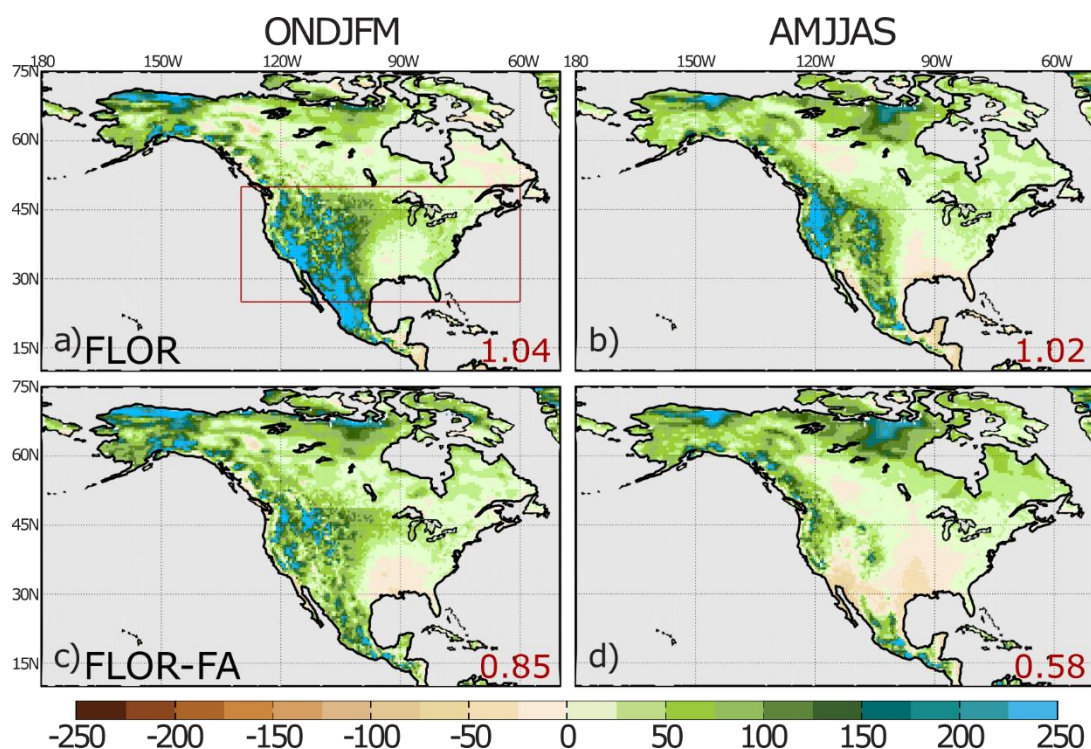


FIG. 5. Climatological precipitation biases (% relative to U. Delaware precipitation) over North America in (top) FLOR and (bottom) FLOR-FA for (a,c) October – March and (b,d) April – September. The values in the lower right corner of each panel are the RMSE (mm d⁻¹) in the U.S. region (red box in a).

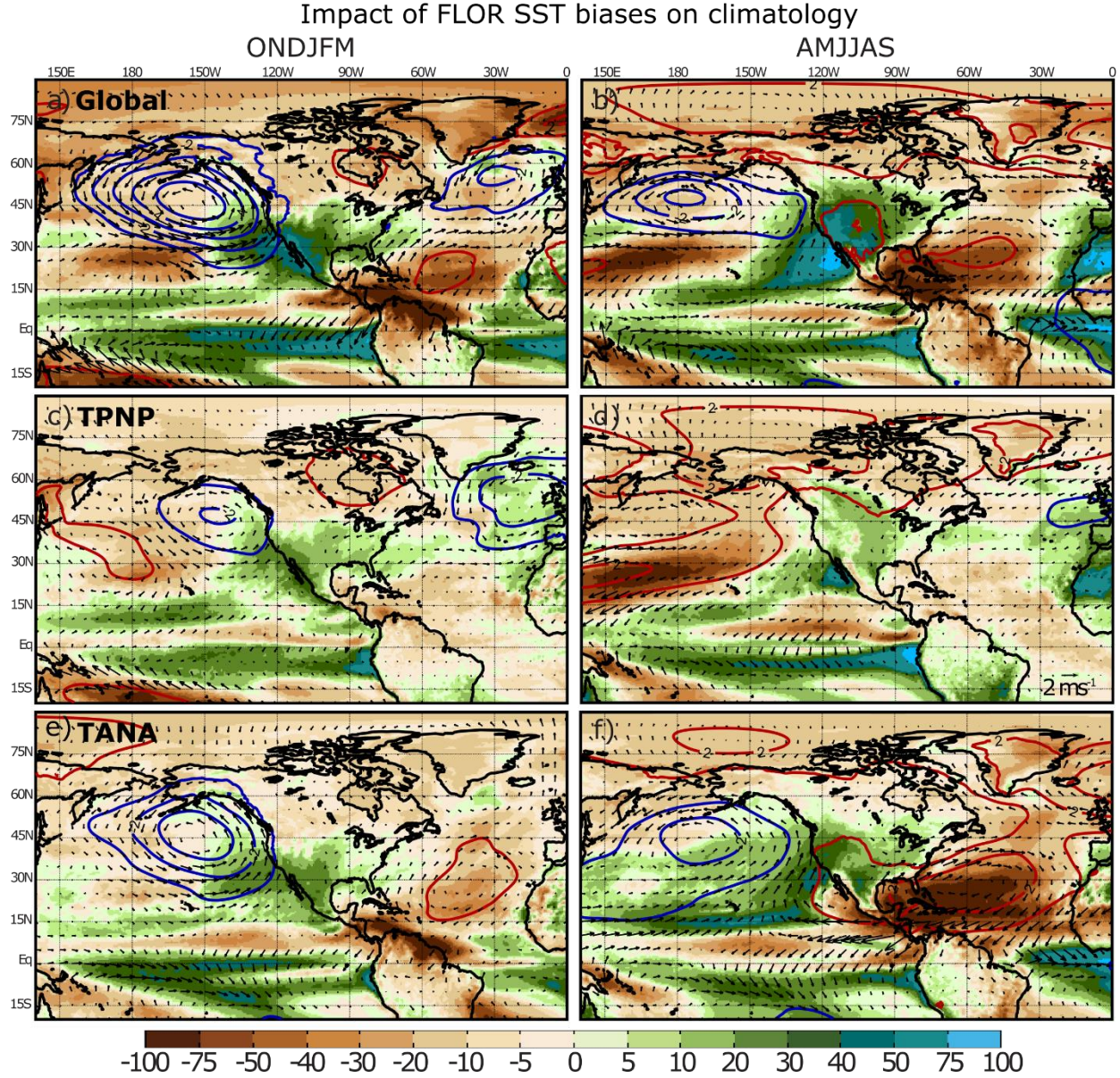


FIG. 6. Impact of (left) October – March and (right) April – September (top) global, (middle) tropical and extratropical Pacific, and (bottom) tropical and extratropical Atlantic FLOR SST biases, including the effects of remotely induced SST biases, as expressed by the (a,b) CTL minus FA, (c,d) CTL minus TPNP, and (e,f) CTL minus TANA climatological differences in precipitation (color shading), SLP (contours), and 925 hPa wind (vectors) for (left) October – March and (right) April – September. Precipitation differences are expressed as percentage relative to CTL climatology. SLP is contoured at intervals of 1 hPa with red (blue) lines indicating

positive (negative) differences, and the zero contour is omitted. The reference vector for 925 hPa wind is shown in the bottom right of panel d.

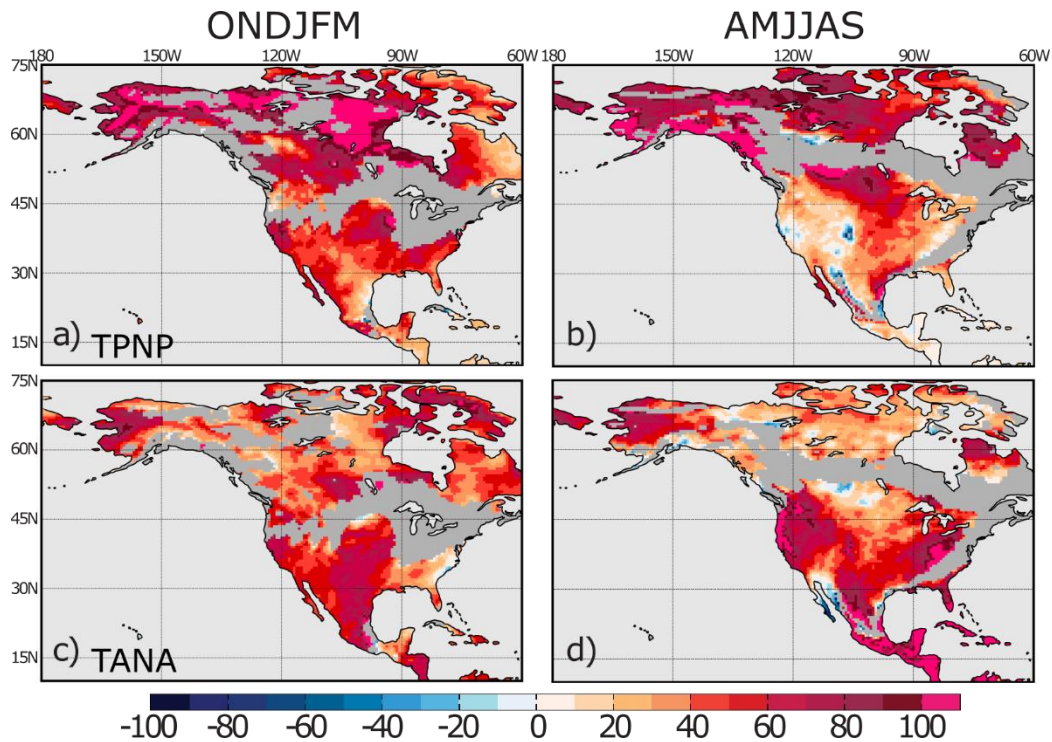
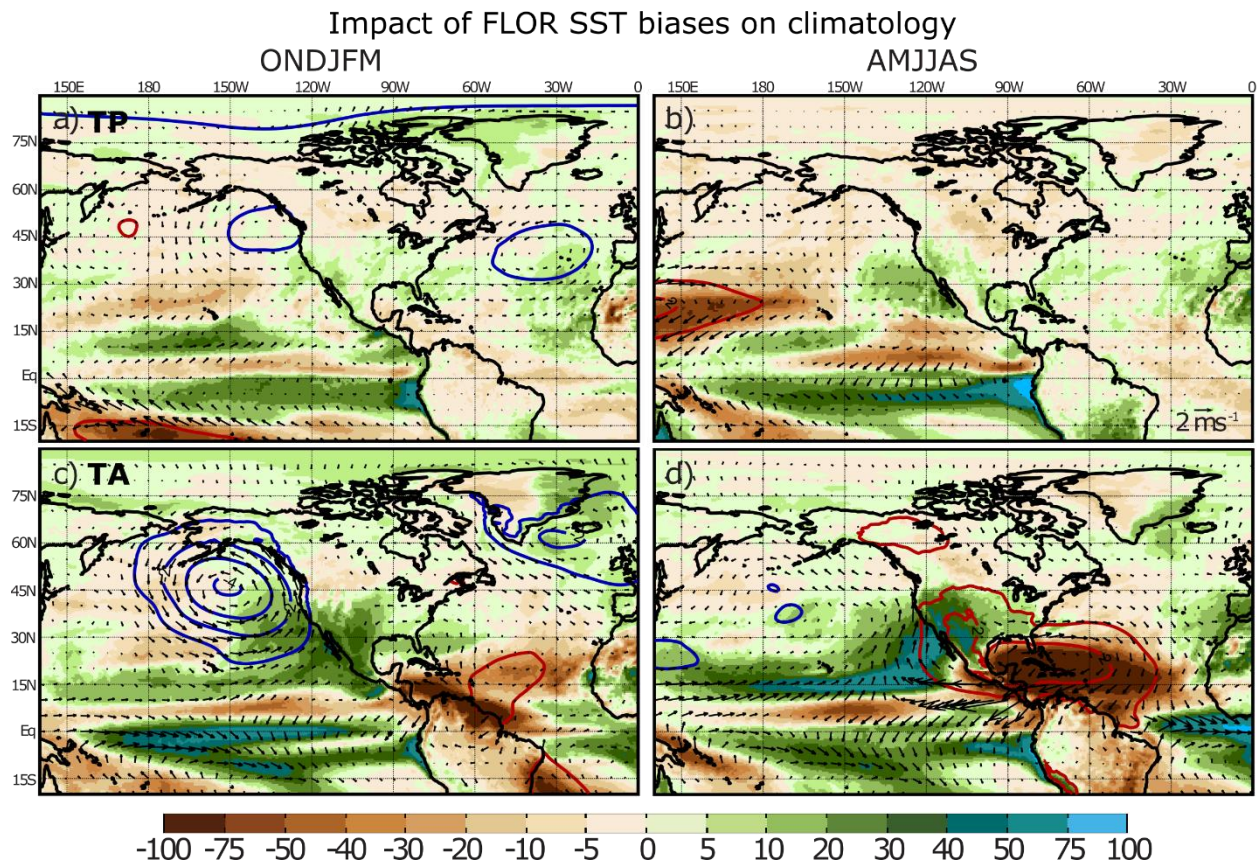


FIG. 7. Percent of $\delta P_{\text{FLOR-FA}}$ that can be attributed to (a,b) TPNP and (c,d) TANA domain SST differences for (left) October – March and (right) April – September. Areas masked in grey represent regions where the FLOR-CTL minus FLOR-FA precipitation differences are less than 10% of the FLOR-CTL climatological precipitation.

1093

1094



1095

1096

1097

1098

1099

1100

1101

1102

1103

1104

FIG. 8. Impact of (top) tropical Pacific and (bottom) tropical Atlantic FLOR SST biases, including the effects of remotely induced SST biases, as expressed by the (a,b) CTL minus TP and (c,d) CTL minus TA climatological differences in precipitation (color shading), SLP (contours), and 925 hPa wind (vectors) for (left) October – March and (right) April – September. Precipitation differences are expressed as percentage relative to CTL climatology. SLP is contoured at intervals of 1 hPa with red (blue) lines indicating positive (negative) differences, and the zero contour is omitted. The reference vector for 925 hPa wind is shown in the bottom right of panel b.

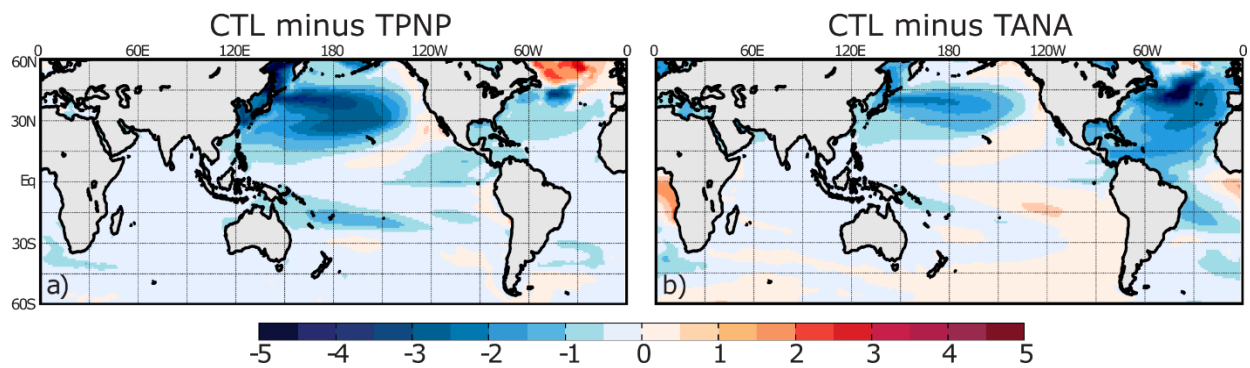


FIG. 9. (a) CTL minus TPNP and (b) CTL minus TANA annual mean climatological SST differences (K).

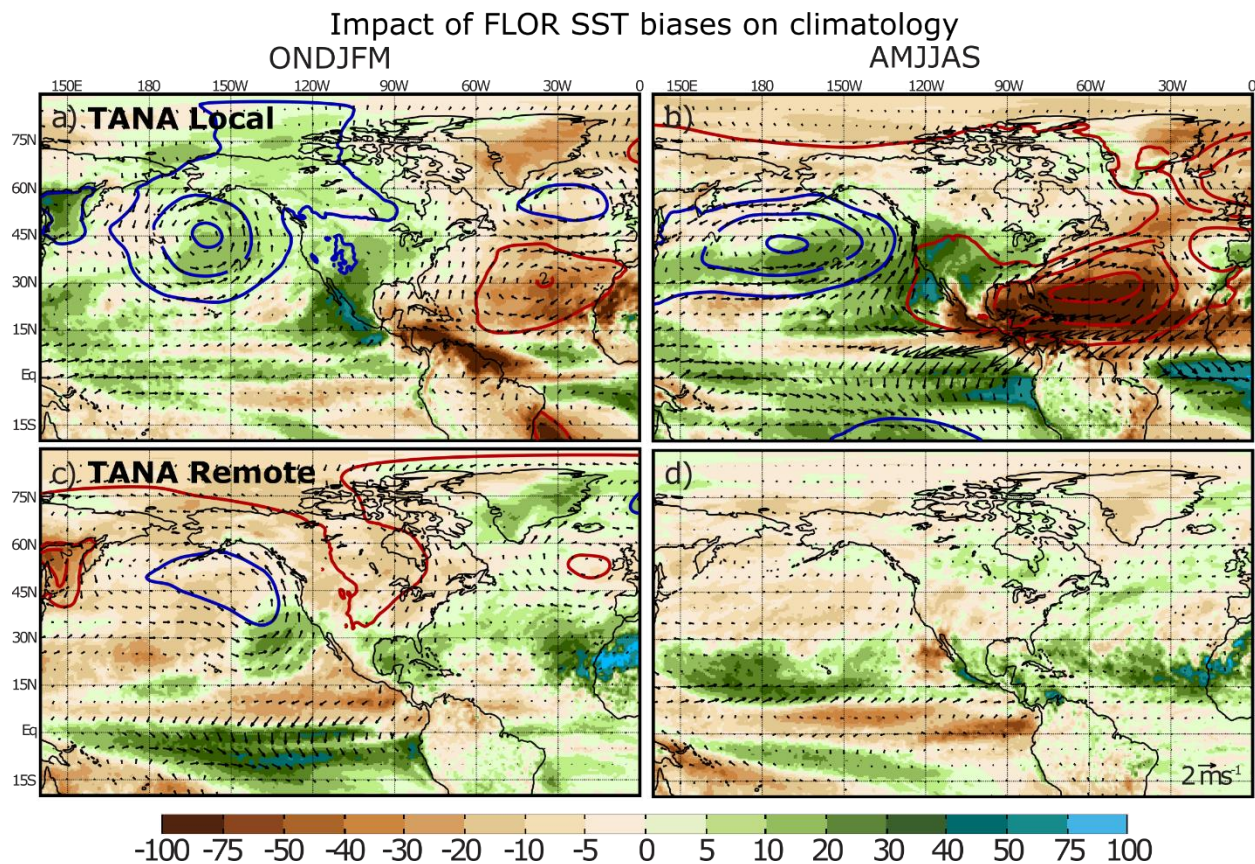


FIG. 10. As in Fig. 8 except for the (a,b) locally forced tropical and extratropical North Atlantic SST effect (CTL minus TANA_{iso}) and the (c,d) remotely forced tropical and extratropical North Atlantic SST effect (TANA_{iso} minus TANA).

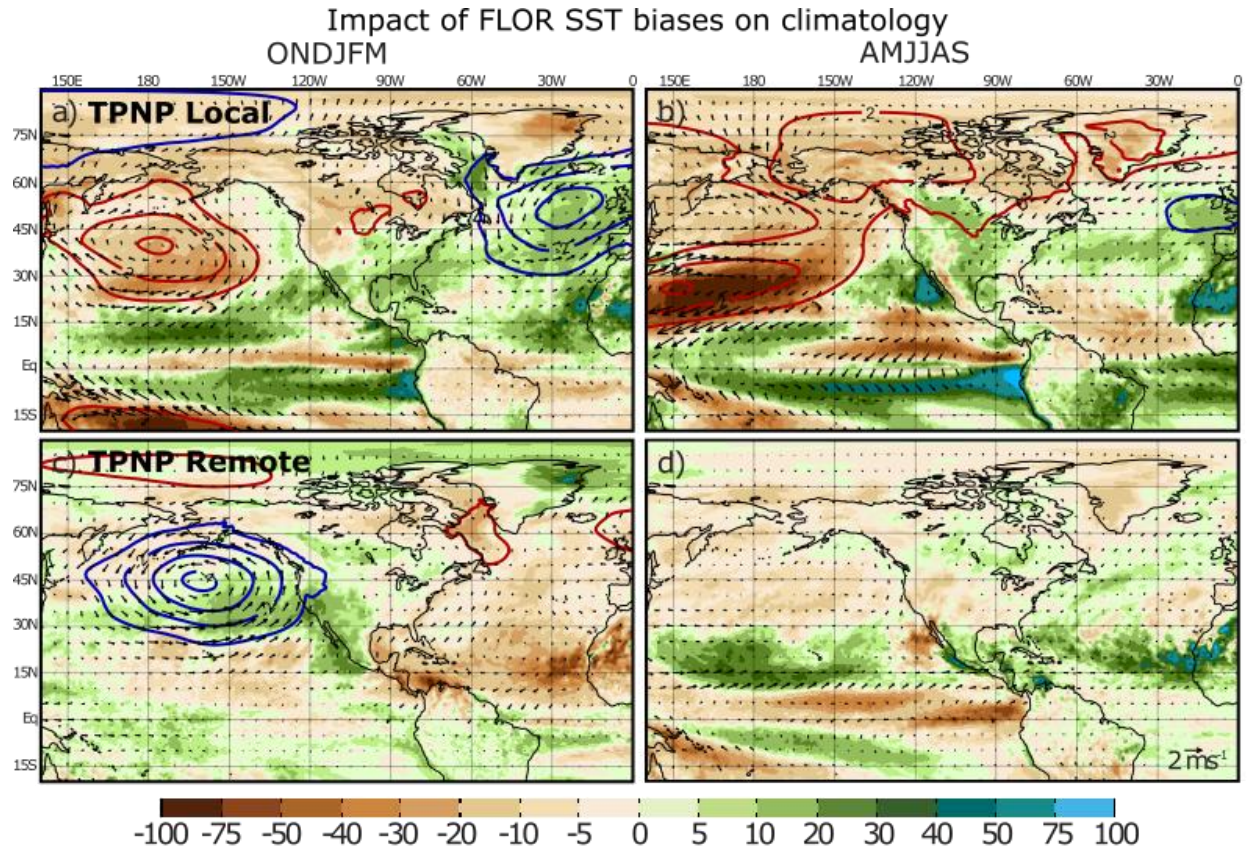


FIG. 11. As in Fig. 8 except for the (a,b) locally forced tropical and extratropical North Pacific SST effect (CTL minus $TPNP_{iso}$) and the (c,d) remotely forced tropical and extratropical North Pacific SST effect ($TPNP_{iso}$ minus TPNP).

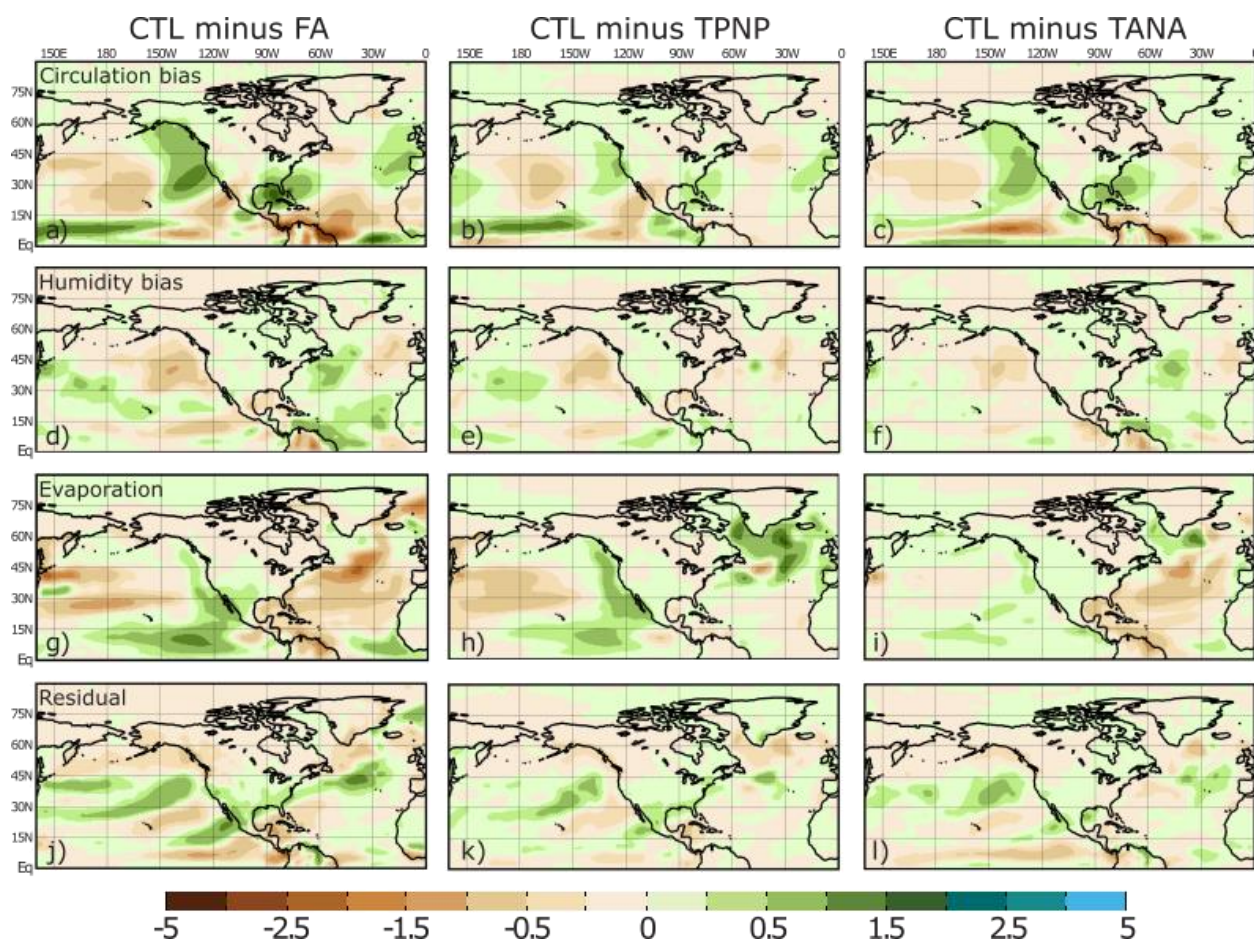
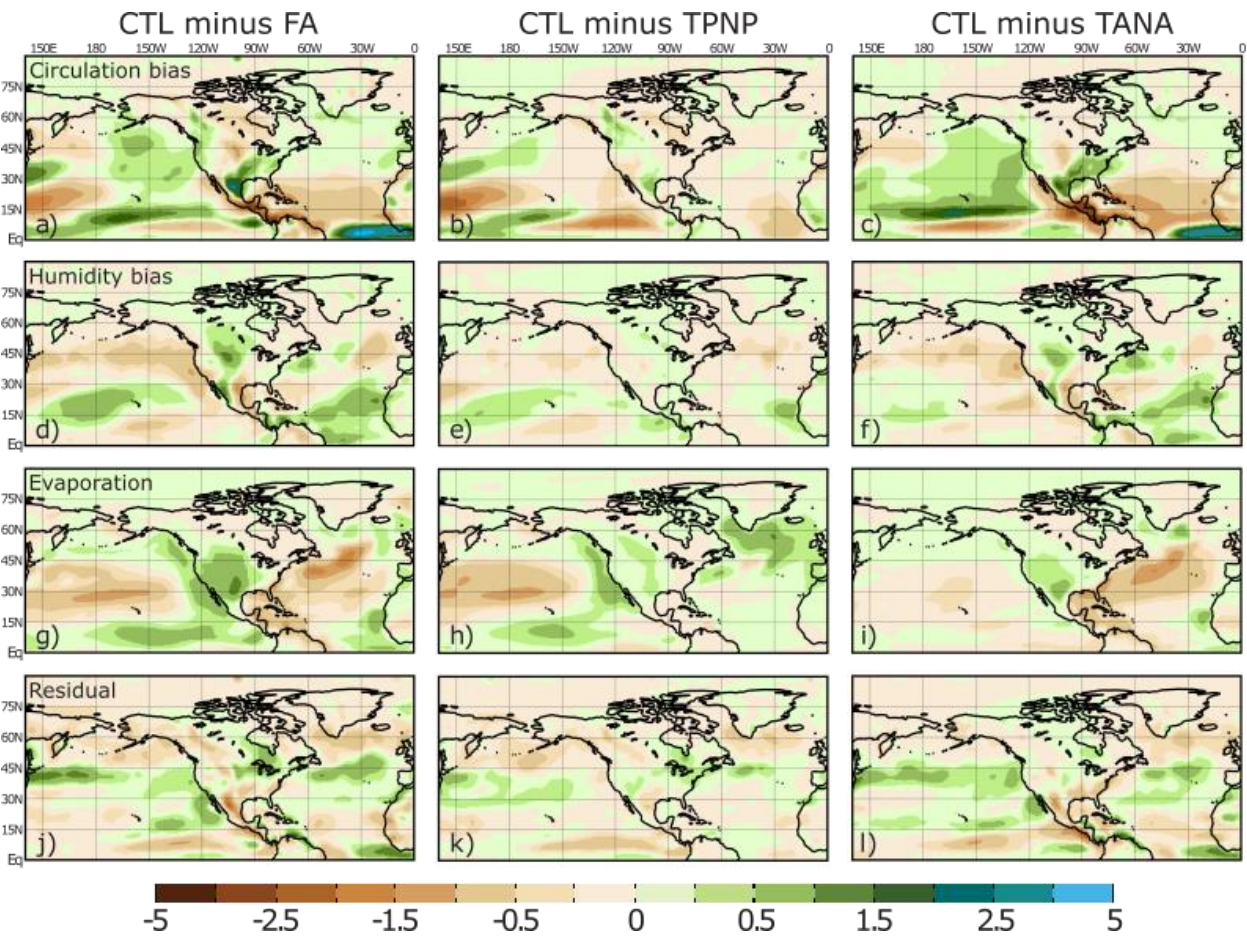


FIG. 12. Contributions to the October – March (left column) CTL minus FA, (middle column) CTL minus TPNP, and (right column) CTL minus TANA climatological precipitation differences (mm d^{-1}) attributed to the following terms: (a-c) circulation bias, (d-f) humidity bias, (g-i) evaporation, and (j-l) the residual, calculated as the actual precipitation difference minus the sum of the three terms.

1146



1147

1148 FIG. 13. As in Fig. 12 but for April – September.

1149

1150

1151

1152

1153

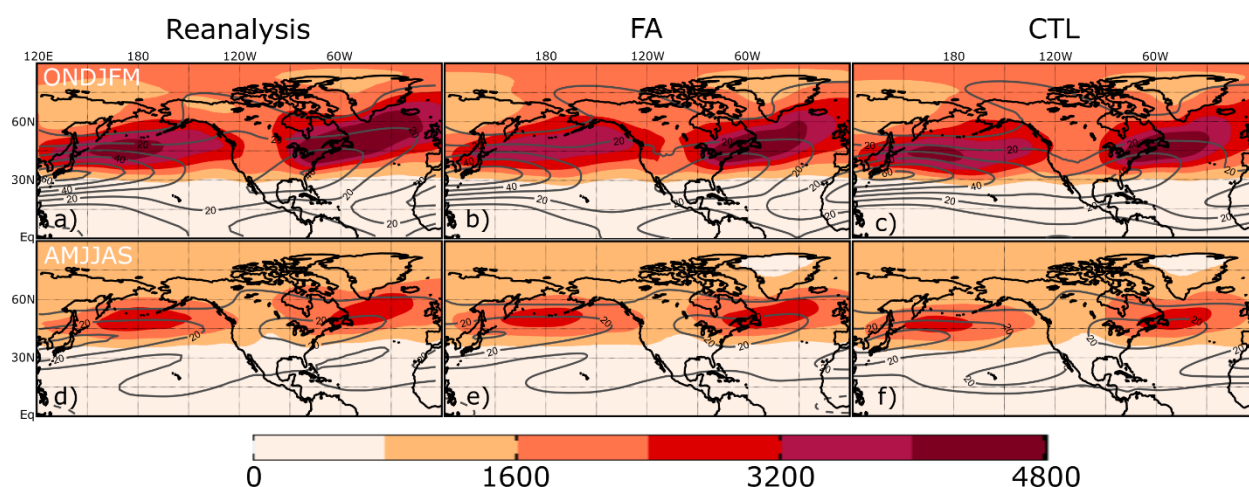


FIG. 14. Climatological storm tracks, as measured by 8-day high-pass filtered 500 hPa geopotential height variance (shading, m^2) and 200 hPa zonal wind (grey contours at an interval of 10 ms^{-1}) for (left) NCEP/NCAR reanalysis data, (center) FA, and (right) CTL simulations in (a-c) October – March and (d-f) April – September.

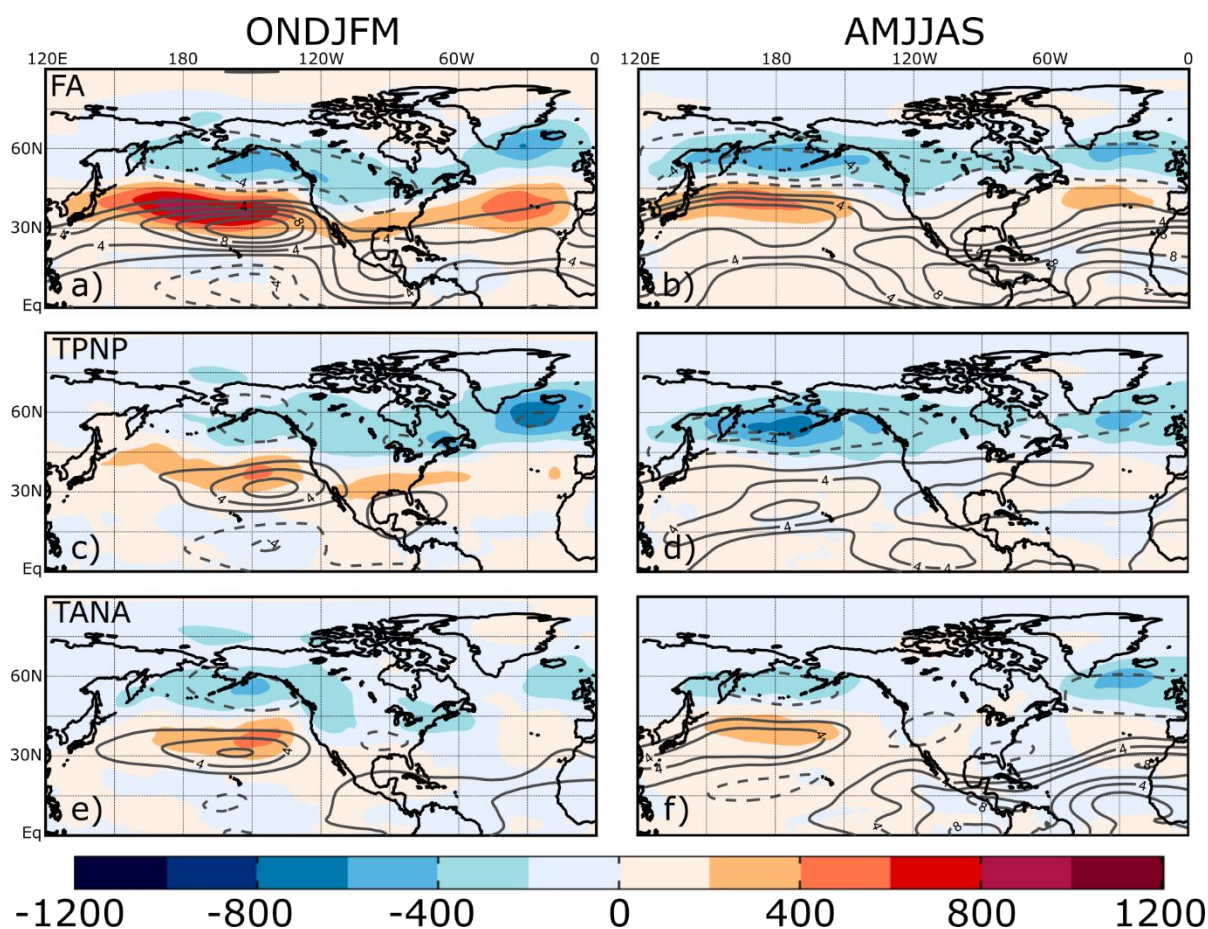
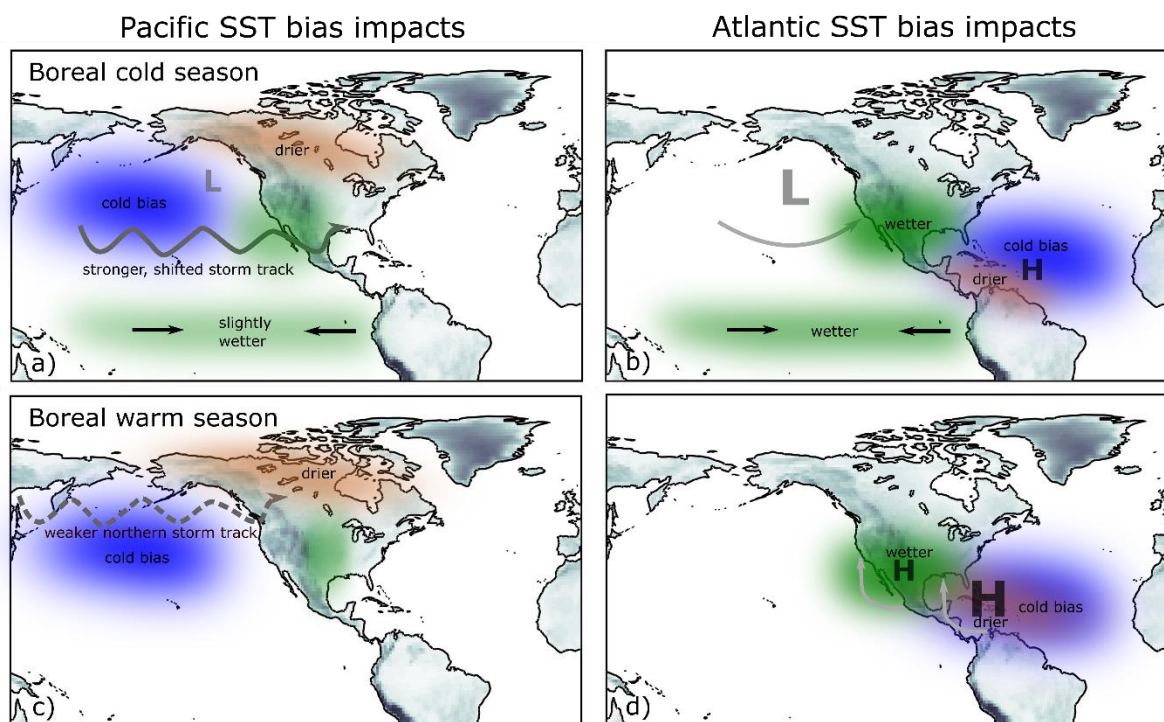


FIG. 15. Differences in climatological storm tracks, as measured by 8-day high-pass filtered 500 hPa geopotential height variance (shading, m^2), and 200 hPa zonal wind (grey contours at an interval of 2 ms^{-1} , zero contour is omitted) for (a,b) CTL minus FA, (c,d) CTL minus TPNP, and (e,f) CTL minus TANA in (left) October – March and (right) April - September.

1174



1175

1176 FIG. 16. Schematic showing the dominant impacts of Pacific and Atlantic SST biases on North
 1177 American precipitation biases in the boreal cold and warm seasons. In the boreal cold season, (a)
 1178 negative SST biases in the extratropical North Pacific promote a strengthened and southerly shifted
 1179 storm track, which enhances precipitation in the southwestern United States and suppresses
 1180 precipitation in northern Canada. (b) Tropical Atlantic cold SST biases induce circulation changes
 1181 throughout the entire tropics resembling the classic Gill model, with a surface anticyclone in the
 1182 vicinity of the cold bias and low-level convergence and enhanced precipitation in the equatorial
 1183 Pacific. The enhanced tropical Pacific rainfall excites a deepened Aleutian low and enhanced
 1184 moisture transport and precipitation in the southern United States. In the boreal warm season, the
 1185 effects of (c) North Pacific SST biases are modest, but a weaker northern portion of the North
 1186 Pacific storm track promotes drier conditions in northern North America. (d) The cold Atlantic
 1187 SST biases have a much stronger impact, substantially strengthening the western lobe of the North

1188 Atlantic Subtropical High and weakening the thermal low over southern North America. These
1189 changes enhance the Great Plains low-level jet and moisture transport into southwestern North
1190 America. Because the SST biases in each basin influence the SST biases in the other basin, the
1191 total SST bias effects are not limited to the direct effects described here.